UNIVERSITY OF CALIFORNIA SAN DIEGO

Insights into Epithelial Cell Senescence from Transcriptome and Secretome Analysis of Human Oral Keratinocytes

A dissertation submitted in partial satisfaction of the
requirements for the degree Doctor of Philosophy

in

Biology

by

Rachael Ellen Schwartz

Committee in charge:

Professor Gerald S. Shadel, Chair
Professor Tony Hunter
Professor Jan Karlseder
Professor Dan S. Kaufman
Professor Cornelis Murre
Professor Robert A.J. Signer

2021

The dissertation of Rachael Ellen Schwartz is approved, and it is acceptable in quality and form for publication on microfilm and electronically:

_____

_____

_____

_____

_____

_____

Chair

University of California San Diego

2021

DEDICATION

To the memory of my grandmother, Josephine, and my mother, Mary Jo, both of whom raised me. And to my brother, John, who cared for me when I was injured.

EPIGRAPH

Life is not easy for any of us. But what of that? We must have perseverance and above all confidence in ourselves. We must believe that we are gifted for something and that this thing must be attained.

Marie Curie

I agree that faith is essential to success in life (success of any sort) but I do not accept your definition of faith, i.e., belief in life after death. In my view, all that is necessary for faith is the belief that by doing our best we shall come nearer to success and that success in our aims (the improvement of the lot of mankind, present and future) is worth attaining.

Rosalind Franklin

Kick out your motor and drive
While you're still alive, kick it out!

Ann Wilson

TABLE OF CONTENTS

LIST OF SUPPLEMENTAL FILES

Supplemental File 1: RNA-seq results

Supplemental File 2: RNA-seq pathways list.

Supplemental File 3: Mass spectrometry results

Supplemental File 4: Proteins in conditioned medium changed with senescence

Supplemental File 5: Proteins in EV pellet changed with senescence

Supplemental File 6: DNA sequencing of EVs from senescent NOKs

LIST OF FIGURES

LIST OF TABLES

ACKNOWLEDGEMENTS

I wish to thank Gerry Shadel and the members of the Shadel Lab at The Salk Institute for Biological Studies for their support, training, and camaraderie. Gerry took me into his lab when I was about to become scientifically homeless due to closure of my initial lab, for which I will always be grateful. Kailash is an encyclopedia of troubleshooting, and was always able to offer multiple solutions to resolve my frustration when my experiments refused to work. Alva is the perfect senescence research buddy: smart, amiable, and the ideal travel companion when attending a distant scientific conference. Laura is immensely knowledgeable about science and generous about sharing that knowledge. And nobody can beat Zheng Hu's combination of friendly enthusiasm and helpfulness.

I am also grateful for the guidance I received from the members of my committee. Their advice always improved my work. Rob initially suggested that I study NOKs. Dan allowed me to work with scientists in his lab to learn NK cell assays, which I expect to use again in the future.

Toshiro Hara, Gerald Pao, Sachin Verma, Xiaoyan Zhu, Eugene Ke, Nina Tonnu, and Nien Hoong of the Verma Lab provided valuable training during my early years as a graduate student, for which I thank them. Many people in the Core facilities at Salk also imparted much-appreciated knowledge, especially Caz O'Connor, who taught me how to do flow cytometry, Max Shokhirev, who gave me many insights into bioinformatics, and Leo Andrade, who skillfully captured the TEM images of extracellular vesicles used herein.

Chapters 1 through 4 and 6 through 7 have been submitted in substantially similar form for publication of the material as it may appear in the journal *Aging.* The input of my co-authors, Max Shokhirev, Leo Andrade, Silvio Gutkind, Ramiro Iglesias-Bartolome, and Gerry Shadel, has been vital. The dissertation author was the primary investigator and author of this paper.

VITA

Bachelor of Arts, Political Science, Johns Hopkins University

Juris Doctor, Georgetown University Law Center

Master of Laws, Corporation Law, New York University

Master of Laws, International Law, New York University

Master of Science, Biotechnology, Johns Hopkins University

Doctor of Philosophy, Biology, University of California San Diego

ABSTRACT OF THE DISSERTATION

Insights into Epithelial Cell Senescence from
Transcriptome and Secretome Analysis of Human Oral Keratinocytes

by

Rachael Ellen Schwartz

Doctor of Philosophy in Biology

University of California San Diego, 2021

Professor Gerald S. Shadel, Chair

Senescent cells are one source of the chronic inflammation associated with the diseases and debilities of aging. Whereas cellular senescence in fibroblasts is well documented, how this process is orchestrated in epithelial cells, the origin of human carcinomas, is much less understood. I used normal primary human oral keratinocytes (NOKs) to elucidate senescence programs in a prototype mucosal epithelial cell that undergoes senescence spontaneously. Widely-accepted assays were used to characterize senescence phenotypes in these cells, and

showed that p21WAF1/CIP1 is not a reliable marker of senescence for NOKs, as it is for fibroblasts. Transcriptome analysis by RNA-seq, and analysis by mass spectrometry of secreted proteins, both soluble and those associated with extracellular vesicles (EVs), were performed. Findings regarding NOK senescence were buttressed using other methods, including microscopy and immunoblotting. Identification of top upregulated and downregulated genes at the mRNA level emphasizes the pro-inflammatory and cancer evasion aspects of NOK senescence. Two of the donors displayed an expected repression of DNA repair genes, correlating with downregulation of E2F1 mRNA and protein, but a divergent result was evidenced for the third donor. Analysis of RNA-seq results within the context of the canonical senescence associated secretory phenotype (SASP) and inflammatory pathways (NF-κB, interferon, and p38MAPK) known to operate in senescence was conducted, and secretion of elements of the canonical soluble SASP was measured. RNA-seq results highlighted potential senolytic targets, including immune evasion mechanisms. The secretome analysis identified a number of pro-inflammatory damage associated molecular patterns (DAMPs) and other molecules that likely contribute to the deleterious effects of senescent cells. The data enabled me to propose additions to the senescence associated secretory phenotype, including HSP60, which was found on the surface of EVs. A co-incubation experiment showed that EVs from senescent NOKs can create inflammation by stimulating STING-dependent interferon pathway signaling in THP-1 monocytes. Sequencing of DNA from these EVs showed that they are associated with mitochondrial and nuclear DNA. These results highlight important senescence changes in epithelial cells in terms of how these cells contribute to chronic inflammation and age-related diseases, and how this inflammation might be alleviated.

INTRODUCTION

The integrity of our DNA is under constant attack. The danger takes multiple forms: oncogenic stress, oxidative stress, telomere erosion, replicative stress, and genotoxic stress (1). These phenomena trigger a DNA damage response (DDR). If the damage is irreparable and the DDR persists, the cell may either engage the apoptosis machinery or enter a state of cellular senescence, as a means to avoid cancer.

Cellular senescence is defined by replicative arrest and adoption of a pro-inflammatory senescence associated secretory phenotype (SASP). The SASP serves to mobilize the immune system toward destruction of senescent cells (2) and tumor cells (3). Natural killer cells, T lymphocytes, macrophages, and neutrophils are recruited by, and their activities on the scene are shaped by, SASP elements (4). Senescence is understood to be an example of antagonistic pleiotropy: beneficial when the organism is young and senescence plays a role in wound healing and tumor suppression, but adverse when the organism is aged (3).

Senescence was originally shown by Leonard Hayflick when he demonstrated, in the 1960's, that fibroblasts do not divide infinitely in culture. This gave rise to the "Hayflick limit," describing the number of replications a cell can undergo. Hayflick's discovery was later found to be a consequence of telomere shortening, due to an inability to fully replicate the lagging strand of DNA on linear chromosomes. The erosion that occurs with each cell division eventually leads to the chromosome end being seen by the cell as a double-strand break, due to a loss of the protective structure at the chromosome ends. Subsequently, additional events that elicit the DDR – such as genomic damage caused by reactive oxygen species or chemicals, excessive mitogenic signaling, and conditions that interfere with DNA replication -- were found to cause senescence (5). Interestingly, some other types of senescence can occur without a triggering of the DDR (*e.g.,* senescence caused by certain kinds of mitochondrial dysfunction) (6).

Profound changes in cell morphology and structure accompany senescence. Cells become larger and flatter. Lysosomes increase in size, due to augmented autophagy (7). The nuclear envelope suffers reduced structural integrity (2). Chromatin architecture is remodeled, such that maintenance of the senescent phenotype is enforced by formation of condensed areas known as senescence associated heterochromatin foci (SAHF). Through use of repressive histone marks, SAHF silence genes whose expression would promote proliferation (7). Some evidence indicates that whereas SAHF are generally found in oncogene-induced senescence, they are not always formed, or take on a different structure, when senescence is induced by other causes (8, 9)

Senescence, in contrast to quiescence, is considered irreversible (10). An exception to this can arise when cells that are already cancerous undergo therapy-induced senescence, by radiation, chemotherapy, or use of drugs (such as inhibitors of cyclin-dependent kinases 4 and 6 or epigenetic modulators) that induce senescence (11). In this event, certain types of cancer cells may reacquire the ability to proliferate (12).

Because the immune system cannot always eliminate senescent cells (13), they endure as the organism ages, serving as a troubling source of persistent inflammation, by virtue of the SASP. Whereas transient inflammation serves productive purposes, such as eliminating pathogenic infections, chronic inflammation is detrimental. Indeed, the major age-associated diseases and debilities, including cancer, heart disease, neurodegenerative diseases, and stem cell dysfunction, each have a substantial inflammatory component (14).

Senescent cells have been found in numerous organs, including brain (astrocytes, microglia) (15), skin (fibroblasts, melanocytes, epithelial cells) (16), the cardiovascular system (endothelial cells) (17) and skeletal muscle (satellite/stem cells) (18). While a foundational understanding of cellular senescence is provided by the excellent work already done, primarily in fibroblasts (10, 19), different cell types display variability in senescence. An understanding of

each of them is essential to development and validation of properly targeted therapeutics (20), such as senolytic treatments that can eliminate senescent cells (21, 22). In recognition of this, the National Institutes of Health Common Fund has established a Cellular Senescence Network (SenNet) Program "to comprehensively identify and characterize the differences in senescent cells across the body, across various states of human health, and across lifespan." (https://commonfund.nih.gov/senescence)

Epithelial cells in particular require study, given that senescence is a cancer avoidance mechanism and most cancers are carcinomas, arising in epithelial tissue. Thus, the work in this dissertation profiles senescence in normal oral keratinocytes (NOKs). NOKs senesce spontaneously over a short time in culture at atmospheric oxygen; however, individual cells in the population senesce at different rates. This allowed characterization of senescence as cells at different stages of the process interact, which is more physiologically relevant than the common approach of inducing senescence simultaneously in an entire population (*e.g.,* by irradiation, chemical treatment, or oncogenic transformation).

NOKs can be obtained from young donors in the process of oral surgery, and are used to study senescence and cancer (23, 24). While there has been some examination of senescence in NOKs, a more robust profile of NOKs senescing spontaneously is needed, both to better understand these cells, particularly given their use in the study of head and neck squamous cell carcinoma, and to explicate epithelial senescence more generally. Existing profiles of senescence in NOKs (25-27) have shed some light on the mechanisms at work. One paper showed that genes highly upregulated at the mRNA level in senescent oral and epidermal keratinocytes were not similarly upregulated in gingival fibroblasts (27), which emphasizes the differences between epithelial and fibroblast senescence. Another provided evidence that certain genes in the pathways of transport, cell proliferation, cell cycle, defense and immune response, transcription, apoptosis, and inflammatory response were upregulated at the mRNA level in

senescent NOKs (25). A third found that NOK senescence is associated with enhanced mRNA expression of certain gene groups, including G-protein-coupled receptors, matrix metalloproteinases, apolipoproteins, and mitochondrial proteins (26). However, these studies relied on the limited microarray technology that was available at the time to assess transcriptional changes, with two of them analyzing only a few thousand genes. They did not analyze the senescent NOK secretome. Nor did they disclose the sex of the donors.

The SASP has been defined primarily in terms of secreted soluble proteins, some of which vary between cell types and the manner in which senescence is induced (19). It is well-known that the soluble SASP is highly dependent on transcriptional activity of NF-κB, particularly in fibroblasts (28). However, this does not mean that NF-κB (or any other transcription factor involved in senescence) promotes transcription of exactly the same target genes in each sort of senescent cell, although certain genes (*e.g., IL6, IL8*) are widely upregulated across cell types (19). Identification of specific components of inflammatory pathways known to participate in the SASP for each cell type can help determine which steps in those pathways might be pharmacologically inhibitable by anti-inflammatory drugs in different cells, in order to achieve a health benefit (29).

Far less is understood about the composition and effects of vesicles released by senescent cells, which may also be considered part of the SASP (22). EVs in senescence include microvesicles and exosomes. Microvesicles (100 to 1,000 nm diameter) bud off the plasma membrane. Exosomes (30 to 150 nm diameter) are formed in multi-vesicular bodies (MVBs) via the endocytic pathway and are released when the MVB fuses with the plasma membrane. Major functions of EVs include disposal of unwanted cellular contents, signaling through receptors on target cells, and transfer of cellular contents between cells (30). The senescing NOK secretome is analyzed here, for the first time.

The role of mitochondria in senescence also deserves further attention. It is known that mitochondria produce much of the reactive oxygen species that inflict senescence-causing oxidative stress (31). It has also been found that mitochondria release their DNA into the cytoplasm under certain kinds of stress (32). Areas that are less understood are the extent to which retrograde signaling from mitochondria to the nucleus might contribute to either senescence or other aging processes (33), and how mitochondrial DNA and proteins might escape from the cell. Research on the latter subject suggests a role for EVs (34).

Efforts to mitigate the deleterious effects of senescent cells have given rise to the field of senolytic research, which is expanding rapidly. Senescent cells are known to simultaneously upregulate expression of both pro- and anti-apoptotic genes (35) and to engage mechanisms that make it more difficult for the immune system to eliminate them (36). Senolytics are therapeutics that are capable of frustrating death evasion strategies by senescent cells. Senolytic therapies currently under study include cancer drugs that inhibit anti-apoptotic proteins (37), existing drugs developed for other purposes that induce pro-apoptotic proteins (38), and modified cytolytic immune cells (39). Care must be taken, however, to avoid collateral damage, such as destruction of healthy cells.

CHAPTER 1 NOKs display increases in established indicia of senescence, excepting p21WAF1/CIP1.

The initial step was to measure NOK performance on a number of tests of senescence that are widely used in the field. Currently, there is no known universal and exclusive marker of senescence (40). Some senescence markers, such as phosphorylated histone H2AX (γH2AX), can be expressed in non-senescent cells, although that mark is removed upon repair of the DSB (41). Quiescent cells, like senescent cells, do not take up EdU. Moreover, beneficial senescence (such as is involved in wound healing) is transitory, but can also be marked by p16INK4A (21).

Accordingly, we utilized multiple assays, applied repeatedly over the entire time course of senescence. With one notable exception, NOKs senesce according to these criteria. The results also formed the basis for selection of which passages to compare in subsequent assessments of changes in NOKs as they progressed through the process of senescence.

1.1 Changes in population growth, morphology, senescence associated β-galactosidase, EdU incorporation, DNA content, γH2AX, and p16INK4A are consistent with senescence.

Cell population growth was measured for six replicates, two from each of 3 donors. (NOK1408 and 1508 were females, aged 18 and 20 years, respectively, and NOK1415 was a male, aged 35 years.) Each replicate attained zero population growth (ZPG), and therefore ceased population doubling, between passages 13 and 16 (Fig. 1.1.1). Given the relatively low number of population doublings before ZPG was reached, compared to the Hayflick limit of approximately 50, it seems unlikely that telomere shortening due to the lagging strand end replication problem was the trigger for NOK senescence (although telomeres are susceptible to oxidative damage) (42). Based on population doublings and the steady decline in growth rate over time, oncogene-induced hyperproliferation also appears improbable as a DDR activator in this case (42).

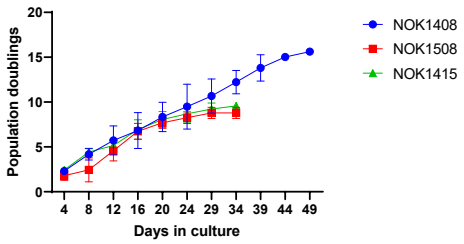

Figure 1.1.1. Population doubling. Y-axis is cumulative population doubling (PD) and X-axis is days in culture starting with passage 5. (Mean of 2 replicates per donor ±SD.) Cumulative PD = 3.322 x [log N(t) – log N(0)] + X, where N(0) is number of cells plated (5 x 10^5), N(t) is number of cells at next passage, and X is PD for prior passages.

Positive staining for senescence-associated β-galactosidase (SAβG), which was performed for four replicates (Donors 1408 and 1415), increased with passaging (Fig. 1.1.2). Morphological changes included enlarged cell size and development of perinuclear vacuoles (Fig. 1.1.2).

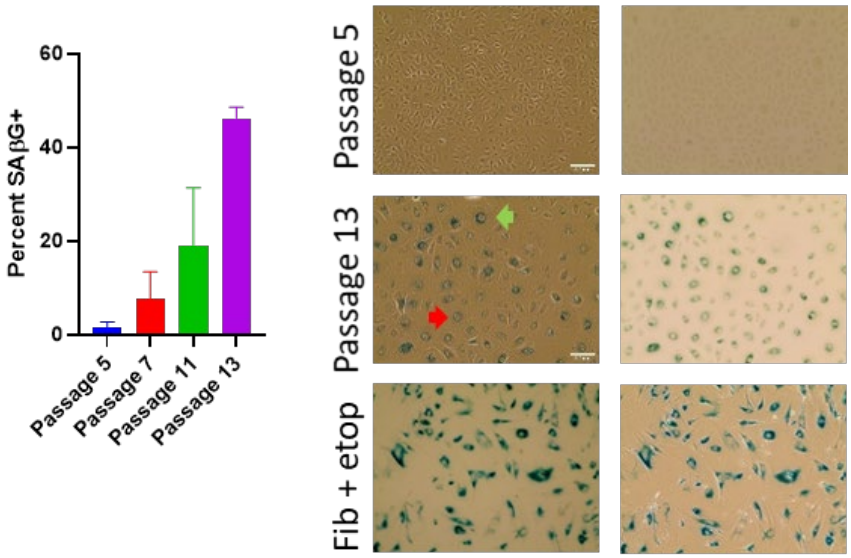

Figure 1.1.2. SAβG+ cells increased with passaging. (Top, passage 5; middle, passage 13, Donor 1415). (Mean ±SD.) Positive control (bottom) is etoposide-treated BJ fibroblasts. (Left, phase contrast; right, brightfield. 20x magnification.) Multinucleate cell, red arrow. Perinuclear vacuoles, green arrow.

Flow cytometry for incorporation of the thymidine analog 5-ethynyl-2 deoxyuridine (EdU) into nuclear DNA, a measure of cell proliferation, revealed a decline in cells staining positive over time. Donors showed a balance of proliferating and non-proliferating cells at passage 10 (Fig. 1.1.3). Analysis of DNA content showed a loss by senescent NOKs of a distinct cell population with the normal diploid content that was seen with proliferating cells (Fig. 1.1.3). This suggests that a portion of NOKs were arrested in a multinucleate state and/or experienced nuclear blebbing of chromatin fragments into the cytoplasm, both of which are features of senescence (43). Staining for phosphorylated histone H2AX (γH2AX), which is generated at DSBs, showed such multinucleate cells and both nuclear and cytoplasmic γH2AX at passage 13 (Fig. 1.1.4). Quantification of combined nuclear and cytoplasmic γH2AX foci demonstrated a significant increase in unrepaired DNA double-strand breaks (DSBs) accompanying senescence (Fig. 1.1.4).

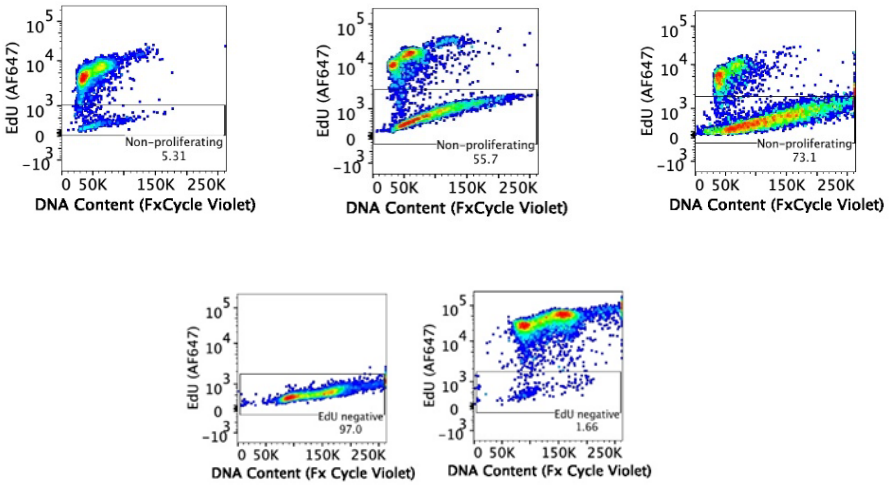

Figure 1.1.3. Representative EdU and DNA content flow cytometry results. Top row, NOK Donor 1415. (Left, passage 5; middle, passage 10; right, last passage.) Bottom row, U2OS cells, no EdU negative control (left) and positive control (right).

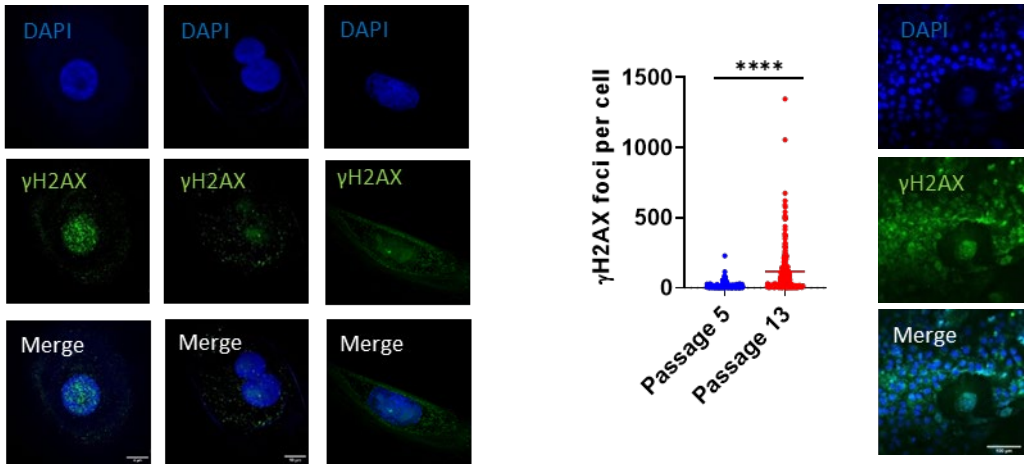

Figure 1.1.4. γH2AX IF. Staining shows significant increase ($p < 0.0001$, two-tailed t-test) in DSBs with passaging (Donors 1415 and 1408, combined), and binucleation and cytosolic foci in passage 13 cells (Donor 1415, left and center column images; Donor 1408, right column images). (Far right, positive control U2OS cells.)

Senescent cell cycle arrest can be mediated by the p16INK4A cyclin-dependent kinase inhibitor (CDKN). Quantified IF for the p16INK4A CDKN significantly increased at passage 13 compared to passage 5 (Fig. 1.1.5).

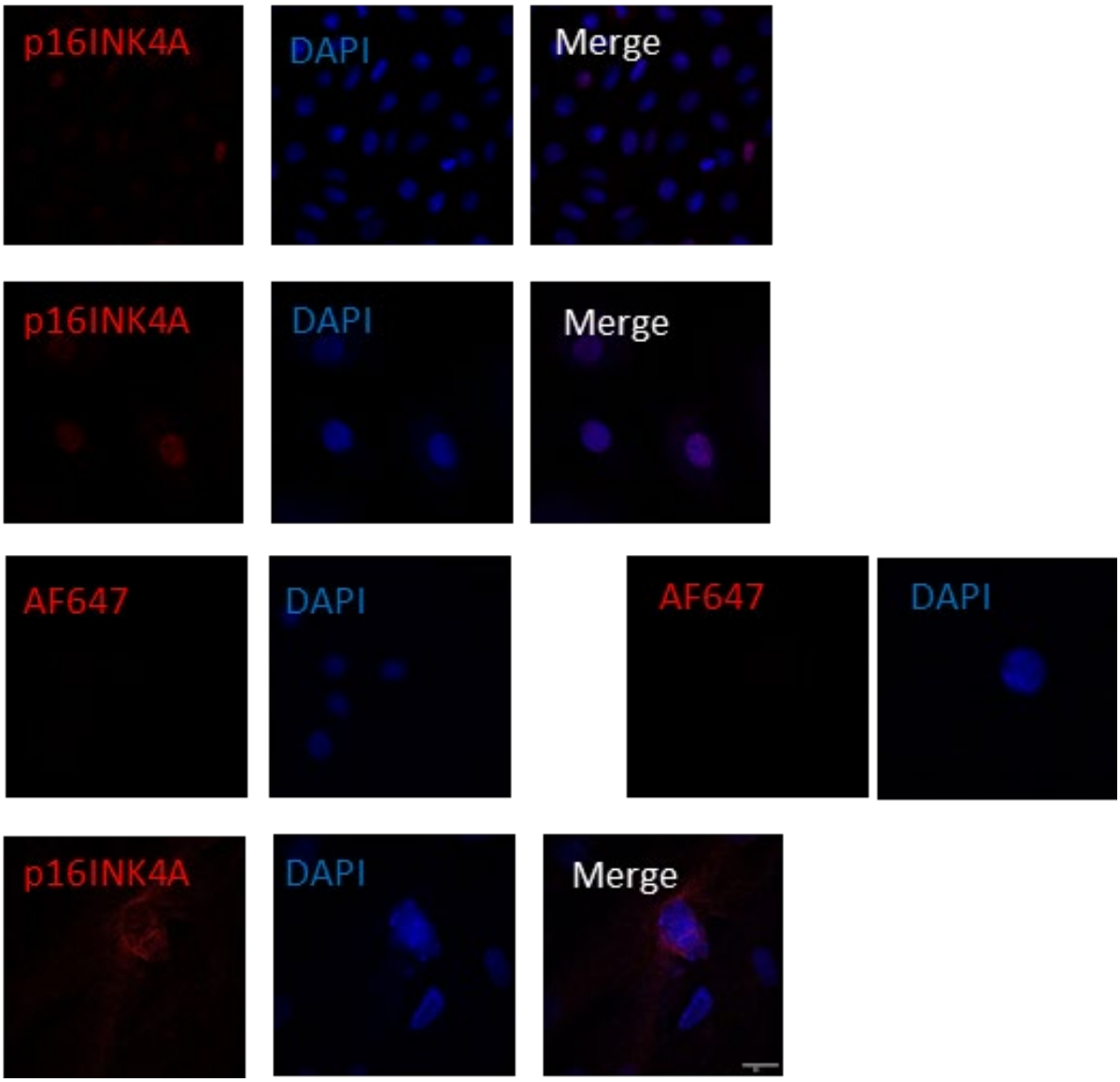

Figure 1.1.5. p16INK4A IF. (Top, passage 5; second row, passage 13). Fluorescence per cell for p16INK4A protein at passage 13 was 2.87 times the level at passage 5 ($p < 0.0001$ using two-tailed t-test) (Donor 1415). IF for p16INK4A negative control NOKs (no primary antibody) (third row left, passage 5; third row right, passage 13) (Donor 1415). IF for positive control etoposide-treated BJ fibroblasts (fourth row).

1.2 p21WAF1/CIP1 is present at early passages and thus is not a reliable marker of senescence in NOKs.

In addition to p16INK4A, the p21WAF1/CIP1 CDKN may also mediate cell cycle arrest. While p21 has long been considered a sign of senescence in fibroblasts (44), 82% of cells stained positive for nuclear p21 at passage 5 (Fig. 1.2.1). Using a different p21 antibody, an immunoblot of whole cell lysate was performed, confirming that p21 was present at early passages and showing that it decreased over time (Fig. 1.2.2). While this means that p21 is not a reliable marker of NOK senescence, it does not allow a conclusion that p21 does not play a role in that process; the multiple functions it performs may change as the cells are passaged. In addition to mediating cell cycle arrest, p21 is active in DNA repair and apoptosis (45).

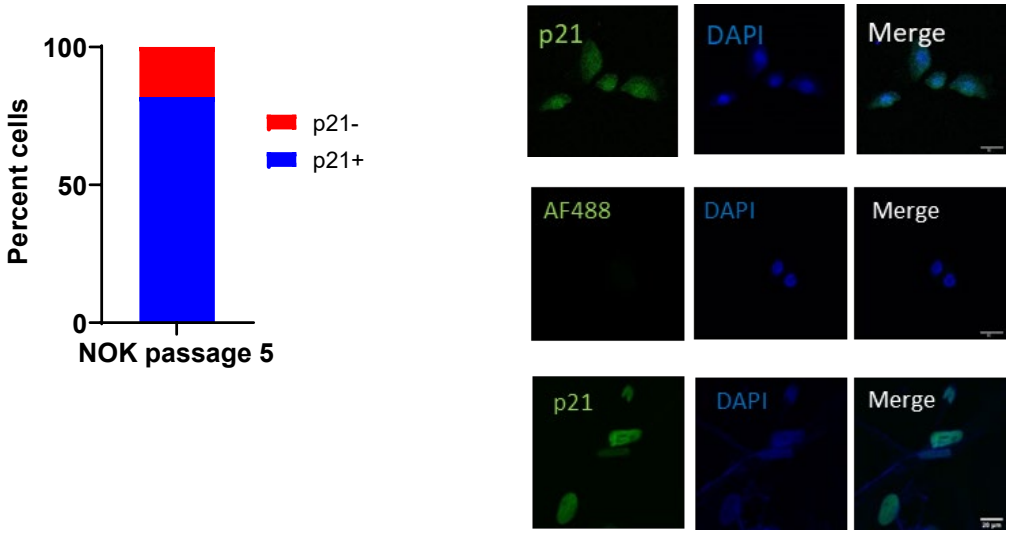

Figure 1.2.1. p21WAF1/CIP1 IF. Cells positive for p21WAF1/CIP1. Percent positive in nucleus at passage 5 (640 total cells from Donors 1408 and 1415). IF shows nuclear p21WAF1/CIP1 protein in passage 5 cells (Donor 1408) (top row), negative control NOKs (no secondary antibody) (middle row), and nuclear p21WAF1/CIP1 protein in positive control etoposide-treated BJ fibroblasts (bottom row).

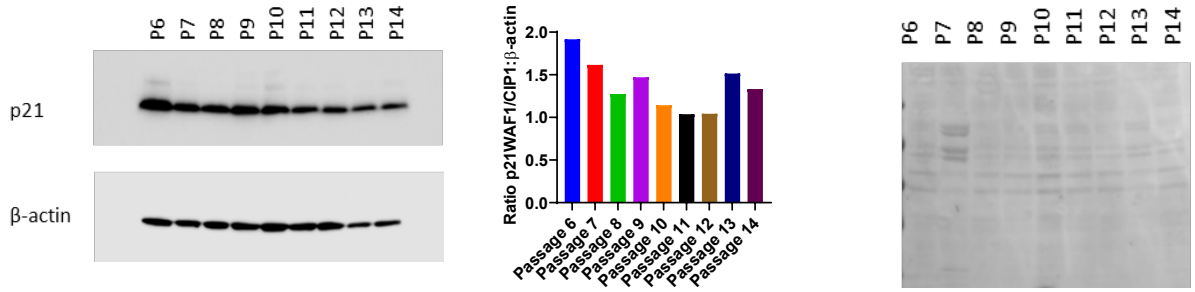

Figure 1.2.2. p21WAF1/CIP1 Immunoblot. Immunoblot (left) shows decline in p21WAF1/CIP1 (NOK1408). p21WAF1/CIP1 ImageJ quantification readings normalized to β-actin (center). Similar results were obtained for normalization to total protein in Ponceau S stain (right).

This evaluation established that NOKs that senesce without irradiation, chemical treatment, or transfection with an oncogene satisfy several criteria of senescence. Some of the assays used, such as measuring population growth and SAβG positivity, have previously been presented as evidence of senescence in such NOKs (25-27, 46). However, the analysis of spontaneous senescence presented here is more comprehensive (*e.g.,* EdU and DNA content flow cytometry, quantification of γH2AX foci). Prior NOK studies have not been in accord on changes in p21WAF1/CIP1 in senescing NOKs. One study found that p21WAF1/CIP1 mRNA increased in senescent cells versus highly proliferating cells (27), another found it nearly unchanged (26), and a third found a significant diminution in p21 protein with senescence (46). The data presented here show that p21 mRNA is transcribed in cultures of largely proliferating, mixed, and majority non-proliferating NOKs (Supp. File 1). p21 protein is also produced at early passages, and declines with senescence. Therefore, p21 is not a trustworthy marker of senescence in NOKs.

Senescence researchers continue to work to identify specific markers of senescence. In particular, a surface marker would allow easy isolation of senescent cells from a diverse population of cells, facilitating further study, as well as a target for therapeutic elimination of

senescent cells. To date, however, these markers have also been found on non-senescent cells (39, 47). If such a marker is found, it is generally believed that it is unlikely to be found on all types of cells that senesce (40).

Chapter 1 has been submitted in substantially similar form for publication of the material as it may appear in the journal *Aging.* The dissertation author was the primary investigator and author of this paper. Co-authors were Max Shokhirev, Leo Andrade, Silvio Gutkind, Ramiro Iglesias-Bartolome, and Gerry Shadel.

CHAPTER 2 Unbiased, global RNA-sequencing of NOK senescence.

RNA-seq results were obtained for each replicate (2 replicates from each of the 3 donors) at passage 5 (majority proliferating), passage 10 (mixed proliferating and arrested), and the final passage (majority arrested) (Supp. File 1). Before examining changes in genes of particular interest, an unbiased analysis of these results was conducted.

2.1 Top 100 upregulated and downregulated genes

The top 100 up and down differentially expressed genes from passage 5 to the last passage were identified. After a stringent p-value cut-off ($p < 0.01$) was applied, the 100 genes with the greatest fold changes were then selected (Fig. 2.1.1 and 2.1.2). The list of top 100 upregulated mRNAs included genes involved in promotion of inflammatory processes (*C3, SPP1, CSF2, CSF3, IL6, NLRP3, CXCL1, CXCL11, S100A7A, CSF1R, C3AR1, TLR4, CCL2, CXCL10, CSFR1, LTB*) or responsive to inflammatory conditions (*FAP, SAA1, SAA2, SAA4, SAA2-4, ANKRD1, MX2*). Others limit inflammation (*TNIP3, SP140*). There were also several proteases (*MME, MMP1, MMP12, MMP10, MMP3, PLAT, ADAM19*) and a protease inhibitor (*TFP12*). Genes whose upregulation is associated with some cancers (*TMEM140, ANXA10, ZNF69, CA9, LOXL2, PAGE3, ELFN1*) were also on this list, as was a putative tumor suppressor (*DEC1*). The dominant theme among the downregulated genes was silencing of genes whose products are upregulated in various cancers. Of the 100 genes, 52 (including some transcribed to non-coding RNAs) have been identified as upregulated in at least one type of cancer. Mixed results have been found for another 10 (*HOTS, EDN2, TGM3, CHL1, SOX21-AS1, ZBTB16, PEG3, ATF3, CCNA1, KCNK7*), which are upregulated in some cancers, but downregulated in others. A third group of downregulated genes includes tumor suppressors and transcription factors for tumor suppressors that are lost or mutated in cancer (*EPHB6, E2F2, KLF2, H19, ZNF750, COX7A1, FOXP2, BMP6, FA2H, BMP8B*). This group included *COX7A1*, a subunit of cytochrome c

oxidase, complex IV of the mitochondrial electron transport chain, suggesting possible downregulation of mitochondrial respiration during NOK senescence.

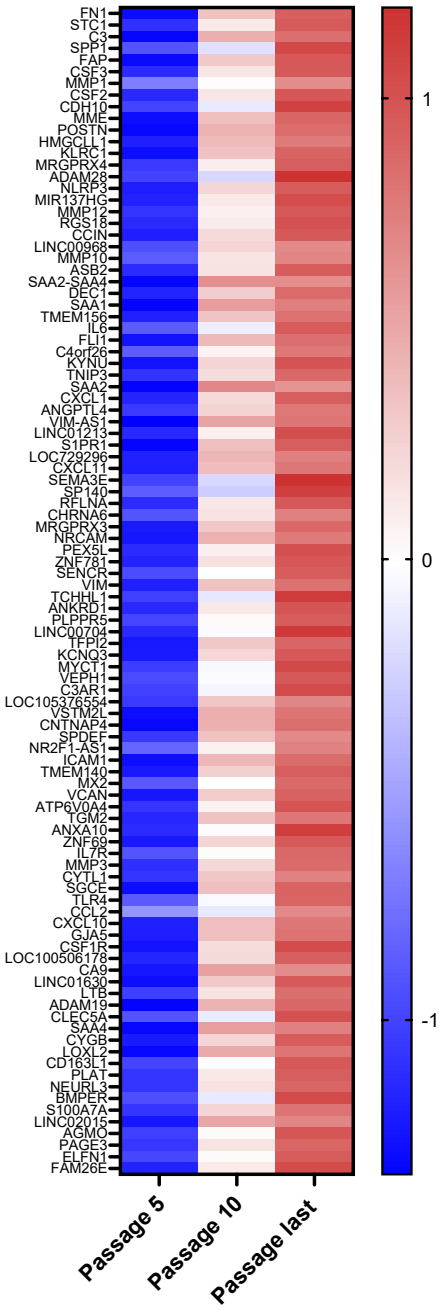

Figure 2.1.1. Top 100 upregulated genes. These include those coding for proteins with functions in inflammation, proteases, protease inhibitors, and genes implicated in cancer.

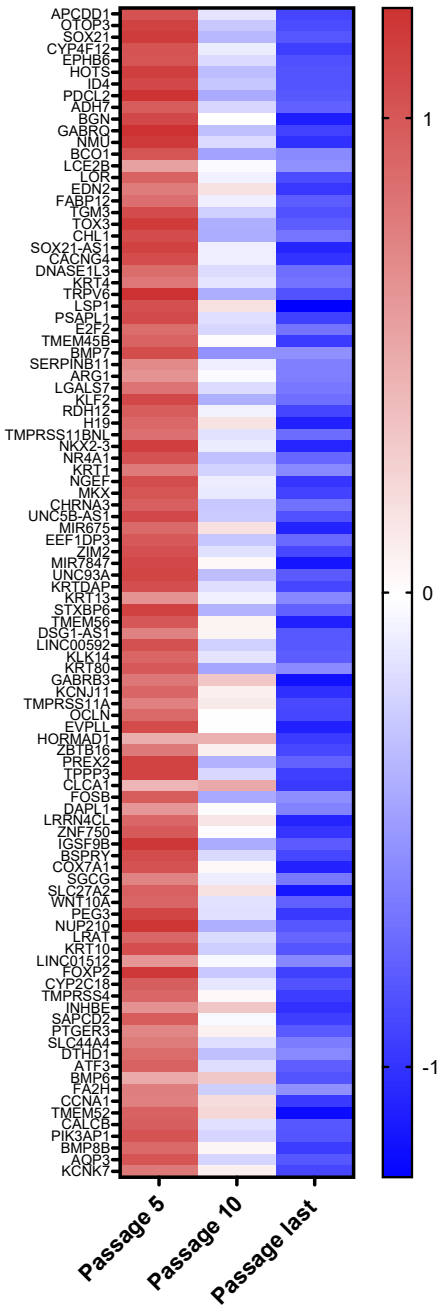

Figure 2.1.2. Top 100 downregulated genes. These include 52 genes upregulated in at least one type of cancer *(ID4, PDCL2, ADH7, BGN, GABRQ, NMU, LCE2B, LOR, FABP12, CACNG4, KRT4, TRPV6, TMEM45B, SERPINB11, ARG1, LGALS7, NKX2-3, NR4A1, KRT1, NGEF, UNC5B-AS1, MIR675, KRTDAP, KRT13, TMEM56, LINC00592, KLK14, KRT80, TMPRSS11A, OCLN, HORMAD1, PREX2, TPPP3, CLCA1, FOSB, DAPL1, LRRN4CL, IGSF9B, SLC27A2, WNT10A, NUP210, KRT10, LINC01512, CYP2C18, TMPRSS4, INHBE, SAPCD2, PTGER3, SLC44A4, CALCB, PIK3AP1, AQP3).*

Some caveats regarding this analysis are in order. If prior studies showing an association between cancer and transcriptional changes used tumor samples from individuals who had received therapy to induce senescence in their cancer cells, that work might actually be showing correlation between senescence and variations in transcription. Moreover, three of the genes on the top 100 lists (*PAGE3, BGN, and GABRQ*) are on the X chromosome and their quantities could be over-represented if dosage compensation were lost in a female donor. Conversely, only one of the three NOK donors was male, and Y chromosome genes, while few in number, could be under-represented in this dataset.

2.2 Principal component analysis

Principal component analysis (PCA) (Fig. 2.2) showed substantial variability among the gene expression patterns of the three donors at passage 5, when most of the cells are actively proliferating. At passage 5, the two female donors were more alike than the third, male donor. However, all of the samples at final passage clustered together and away from the passage 5 samples. This convergence at the final passage, where senescent cells had accumulated, suggests commonality, but not complete identity, in the senescence gene expression signature.

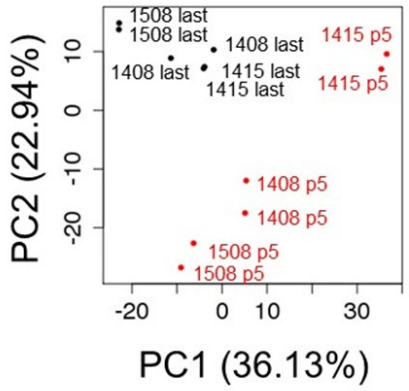

Figure 2.2. Principal component analysis. Passage 5 and last passage for each replicate.

2.3 Gene Ontology pathways

Gene Ontology (GO) overrepresentation analysis using WebGestalt revealed that senescence brings upregulation of inflammatory pathways, including responses to IFN, and downregulation of peptide cross-linking, which is needed to stabilize proper protein folding (Fig. 2.3.1). Interim comparisons (Fig. 2.3.2 &.2.3.3) show similar pathway changes, with the exception that elements of the acute inflammatory response were downregulated at last passage compared to passage 10. The seven acute inflammatory response genes that were downregulated for this interim comparison (*NUPR1, ADAM8, CFB, CXCR2, TREM1, TNFSF11, and PRGER3*), however, were largely different from the inflammatory genes that were upregulated when comparing the last passage to passage 5.

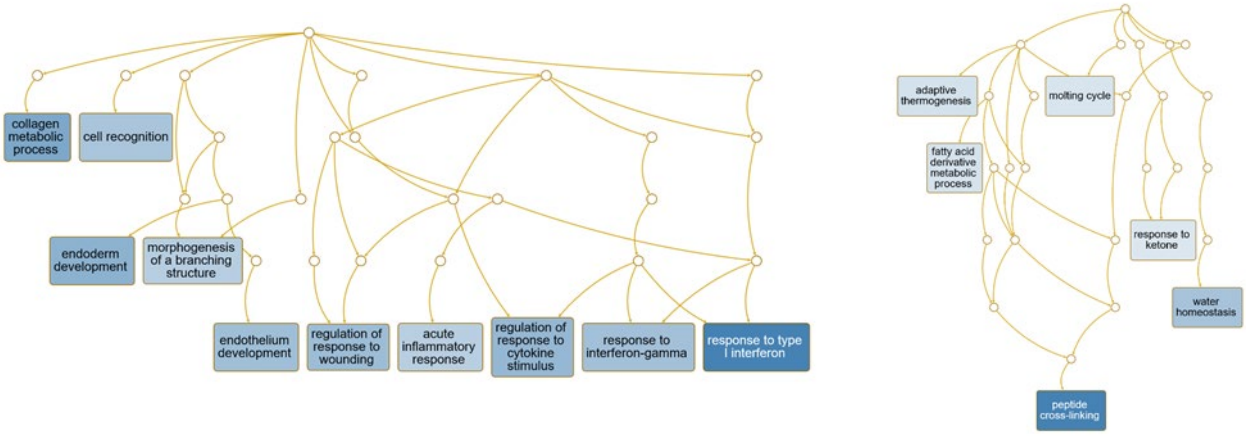

Figure 2.3.1. GO analysis passage last vs passage 5. Inflammatory processes are upregulated (left). Peptide cross-linking is downregulated (right).

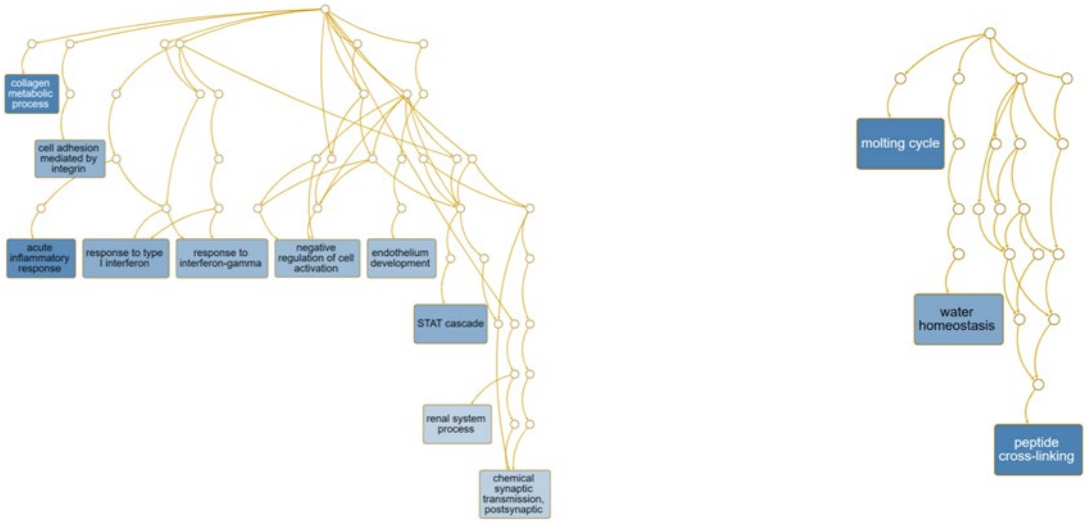

Figure 2.3.2. GO analysis passage 10 vs passage 5. Inflammatory processes are upregulated (left). Peptide cross-linking is downregulated (right).

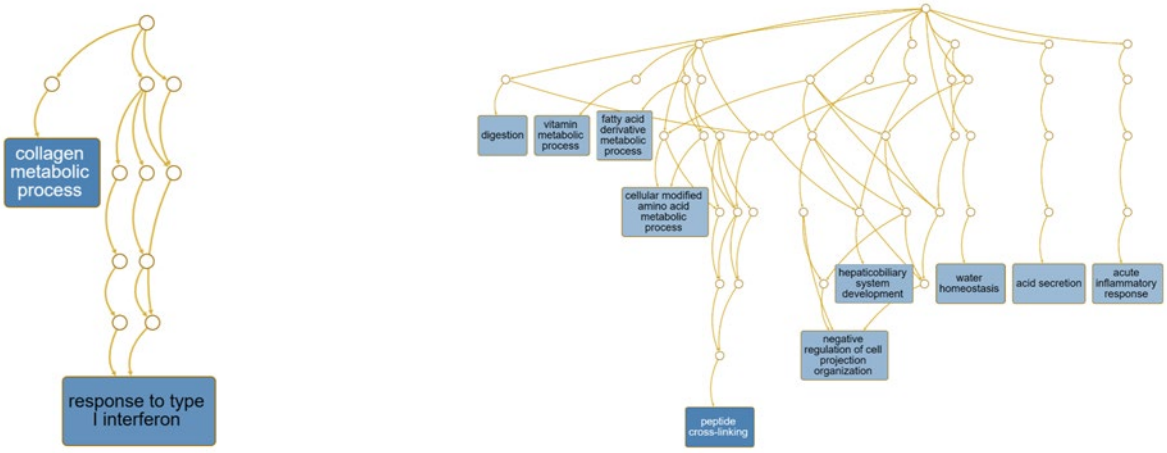

Figure 2.3.3. GO analysis passage last vs passage 10. Type I interferons are upregulated (left). Acute inflammatory response is downregulated (right).

2.4 HOMER analysis

HOMER (Hypergeometric Optimization of Motif EnRichment) *de novo* motif enrichment software was used to identify the transcription factors most likely responsible for the changes in mRNA observed with senescence. HOMER identifies known transcription factor binding motifs in the promoter regions of the genes from which those mRNAs are transcribed. An examination of genes that were significantly changed ($p < 0.05$) up or down at passage 10 vs passage 5, last passage vs passage 5, and last passage vs passage 10 was conducted. The goal in conducting both final and interim comparisons was to distinguish changes that occurred along the entire process of senescence from those that were limited to a period when cells were mostly proliferating or senescent. Applying an FDR of 0.05, three of these six searches produced results: up in last passage vs passage 5, down in last passage vs passage 5, and down in passage 10 vs passage 5 (Fig. 2.4). Comparing the last passage to passage 5, HOMER identified 3 motifs among the upregulated genes and 5 motifs among the downregulated genes. Promoters of genes that were upregulated were enriched in binding sites for NF-κB and the IFN stimulated response element (ISRE). Of the five motifs in downregulated genes, the top hit was for Smad3. Smad3 activity is negatively regulated by cyclin D1 (48); an increase in cyclin D1 is a hallmark of senescence and was seen in senescent NOKs (Supp. File 1). Some motifs appeared only when comparing genes downregulated at passage 10 versus passage 5. One was the CCAAT-box. Among the transcription factors binding this motif is nuclear factor Y, whose target genes are involved in cell cycle progression and DNA repair (49). Two of the motifs are rich in guanine bases, which are susceptible to reactive oxygen species-induced 8-oxoG DNA lesions that may hinder transcription factor binding (50).

	Motifs Enriched in Promoters of Upregulated Genes (Passage last vs passage 5)	q-value/FDR	% of Targets	% of Background	Best Match/Details
1		0.001	1.35%	0.05%	NFkB-p65-Rel(RHD)/ThioMac-LPS-Expression(GSE23622)/Homer(0.917)
2		0.001	6.67%	2.30%	Fra1(bZIP)/BT549-Fra1-ChIP-Seq(GSE46166)/Homer(0.733)
3		0.003	2.98%	0.57%	ISRE(IRF)/ThioMac-LPS-Expression(GSE23622)/Homer(0.941)

	Motifs Enriched in in Promoters of Downregulated Genes (Passage last vs passage 5)	q-value/FDR	% of Targets	% of Background	Best Match/Details
1		0.015	0.77%	0.00%	PB0060.1_Smad3_1/Jaspar(0.738)
2		0.043	2.13%	0.28%	E2F7(E2F)/Hela-E2F7-ChIP-Seq(GSE32673)/Homer(0.800)
3		0.043	2.13%	0.29%	TATA-Box(TBP)/Promoter/Homer(0.621)
4		0.003	9.86%	4.75%	POL012.1_TATA-Box/Jaspar(0.896)
10		0.004	13.01%	7.31%	FOXL1/MA0033.2/Jaspar(0.846)

#	Motifs Enriched in Promoters of Downregulated Genes (Passage 10 vs Passage 5)	q-value	% of Targets	% of Backgrounds	Best Match
1		0.002	3.83%	0.10%	Gata1(Zf)/K562-GATA1-ChIP-Seq(GSE18829)/Homer(0.655)
2		0.007	5.43%	0.39%	TBP/MA0108.2/Jaspar(0.725)
3		0.016	2.56%	0.02%	USF1/MA0093.2/Jaspar(0.757)
4		0.025	5.43%	0.49%	AP-2alpha(AP2)/Hela-AP2alpha-ChIP-Seq(GSE31477)/Homer(0.748)
5		0.025	3.51%	0.12%	PB0165.1_Sox11_2/Jaspar(0.710)
6		0.025	2.24%	0.01%	POL004.1_CCAAT-box/Jaspar(0.675)
7		0.025	3.83%	0.17%	MF0005.1_Forkhead_class/Jaspar(0.758)
8		0.043	7.03%	0.98%	PB0056.1_Rfxdc2_1/Jaspar(0.732)
9		0.025	3.19%	0.10%	Brn2(POU,Homeobox)/NPC-Brn2-ChIP-Seq(GSE35496)/Homer(0.665)
10		0.035	2.88%	0.07%	MEF2A/MA0052.3/Jaspar(0.815)
11		0.036	1.60%	0.00%	KLF4/MA0039.3/Jaspar(0.711)

Figure 2.4. HOMER transcription factor motif analysis. Top: Analysis for genes upregulated with senescence comparing last passage to passage 5 shows binding sites for pro-inflammatory transcription factors. Middle: Analysis for genes downregulated with senescence comparing last passage to passage 5 includes Smad3 binding site and two TATA-box sequences. Bottom: Analysis for genes downregulated comparing passage 10 to passage 5. (FDR = 0.05, showing only the best match for each motif).

There was also a change in mRNA for some transcription factors that bind these motifs. Comparing the last passage to passage 5, mRNA was significantly upregulated for *STAT1*, *STAT2*, and *IRF9* (Supp. File 1), which bind the ISRE. Conversely, *MEF2A* and *KLF4* mRNA were significantly downregulated from passage 5 to passage 10 (Supp. File 1). The fact that mRNA for many of the transcription factors whose binding motifs were identified by HOMER was largely unchanged suggests that the abundance and/or activity of these factors are regulated at a different level. For example, activity of the NF-κB subunit p65 is known to depend on destruction of its inhibitor, IκB, and on subsequent phosphorylation and acetylation of p65.

2.5 DNA repair

Since downregulation of DNA repair genes has previously been observed in senescence (51), it was surprising to find only a weak trend toward downregulation of these genes in the NOK dataset. When the data was broken down by donor, it became clear that elements of several DNA repair mechanisms were significantly down for the two female donors (Donors 1408 and 1508) (Fig. 2.5.1), but the pattern was in the opposite direction for the male donor (Donor 1415) (Fig. 2.5.1). There was, however, an increase in mRNA for DNA polymerase mu (*POLM)*, which participates in non-homologous end-joining (NHEJ), for all three donors (Fig. 2.5.1). *E2F1*, a key transcription factor in DNA repair (51), was one of the genes demonstrating the divergent pattern at the mRNA level (Supp. File 1). Corresponding with the mRNA, the amount of E2F1 protein decreased with senescence for one of the female donors (Fig. 2.5.2), but increased with senescence for the male donor (Fig. 2.5.2). The multiple bands on the blots are likely due to alternatively spliced versions of the protein (52). IF staining of cells for Rad51, the protein product of another DNA repair gene that showed the divergent, donor-specific pattern at the mRNA level (Fig. 2.5.3), was also performed. Rad51 mediates the repair of DNA DSBs by facilitating homologous recombination (53). Although average fluorescence per cell increased with senescence for both the male (NOK1415) and female (NOK1508) donors, the increase was much

stronger for the male donor compared to the female donor. Rad51 fluorescence increased four-fold for the male donor, but only 50% for the female donor, comparing passage 13 to passage 7 (Fig. 2.5.3). The greater increase in protein for the male donor is consistent with the increase in RAD51 mRNA for that donor. The results for the female donor suggest that post-transcriptional mechanisms lead to some increase in the amount of Rad51 protein, despite downregulation of the mRNA.

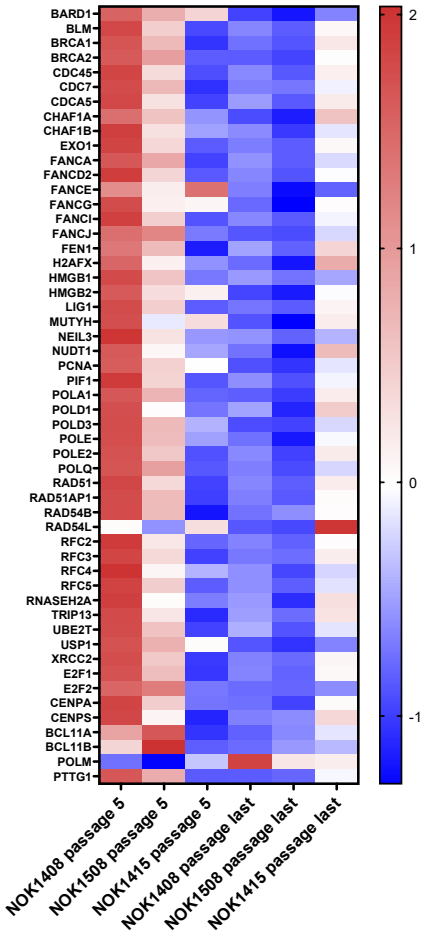

Figure 2.5.1. Heat map by donor of DNA repair genes. Z-scores for genes involved in DNA repair whose mRNA was significantly downregulated (adj. p-value < 0.05 comparing last passage to passage 5) for the two female donors, plus polymerase μ (second from bottom), which was significantly upregulated.

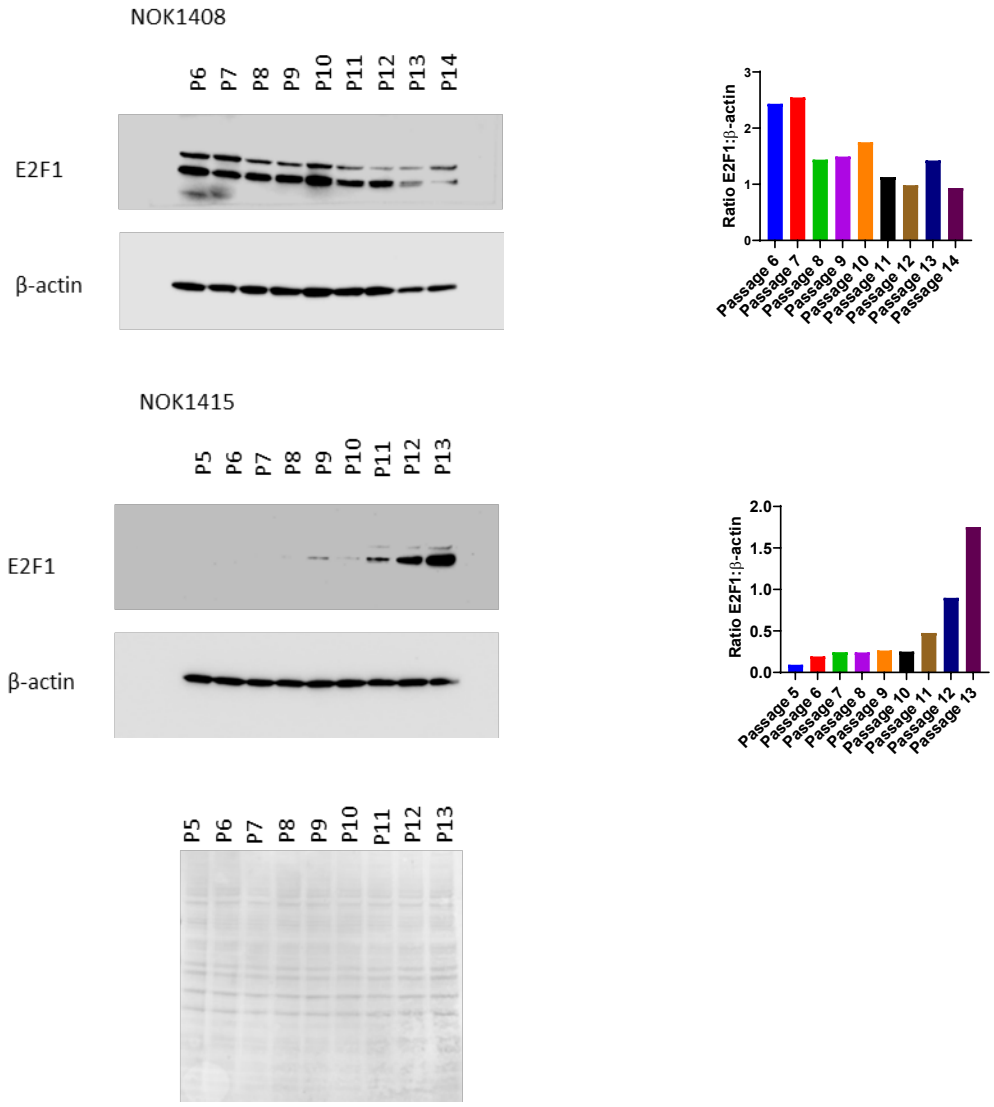

Figure 2.5.2. Immunoblotting for E2F1. Protein decreases with senescence for a female donor (Donor 1408, top blot and bar chart), but increases for male donor (Donor 1415, bottom blot and bar chart). Similar results were obtained for normalization to total protein. (Ponceau for total protein for Donor 1408 in Fig. 1.2.2. Ponceau for total protein for Donor 1415, above.)

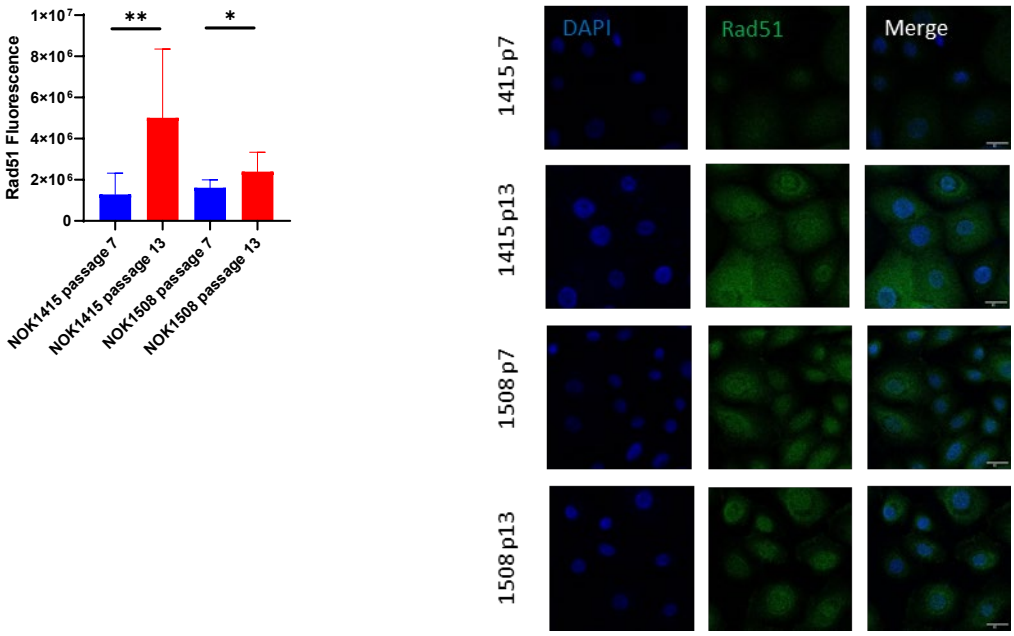

Figure 2.5.3. Change with senescence in Rad51 IF. Quantification of fluorescence (left, p-values determined using two-tailed t-test) and representative images (right).

Sex differences in DNA repair capacity and consequent susceptibility to certain cancers have previously been observed (54). Thus, the divergent trend may be most relevant when the senescence machinery is unable to enforce replicative arrest of potentially cancerous cells (55). Based solely on a comparison of three donors, it is not possible to attribute the differences in transcription and protein for DNA repair genes to sex, or to some other factor specific to a donor. However, the matter bears further investigation and underscores the importance of studying cells and organisms exhibiting diverse traits.

2.6 Comparison to core signature of senescence

The RNA-seq results were compared to those from a study of various cell types induced to senesce by DNA damage, telomere shortening, and oncogenic transformation, in order to extract a core signature of senescence (16). That study identified 55 genes significantly changed at the mRNA level in each cell type examined and for each method by which senescence was

induced. The list of genes significantly changed with NOK senescence showed an overlap with this core signature of 29 genes: 16 genes (*ADPGK, B4GALT7, CCND1, DDA1, DGKA, FAM214B, GDNF, P4HA2, PDLIM4, PLXNA3, POFUT2, RAI14, SLC16A3, TAF13, TMEM87B, ZNHIT1*) were significantly upregulated in both data sets, 12 genes (*ARHGAP35, ARID2, C2CD5, CREBBP, MEIS1, NFIA, PCIF1, RHNO1, SPATA6, SPIN4, STAG1, USP6NL*) were significantly downregulated in both, and one (*BCL2L2*) was up in the core signature but down in NOKs. The genes conserved between the two data sets are involved in a range of processes, including transcription, apoptosis, cell cycle, and cell growth. Cyclin D1 (*CCND1*), for example, prevents entry into S-phase [44]. Some (e.g., *GDNF*) have been found to be associated with cancer. Of particular interest is that transcription of the *BCL2L2* gene was increased with senescence in the core signature, but decreased in NOKs. This implies that a senolytic treatment that would be effective in other cells by virtue of inhibiting Bcl-2-like protein 2 would not induce apoptosis in senescent NOKs. Transcription of another anti-apoptotic gene, *BCL2A1*, however, was significantly upregulated in NOKs. Changes in mRNA levels of anti-apoptotic members of the *BCL2* family in senescing NOKs are discussed in more detail in Section 5.1, below.

Chapter 2 has been submitted in substantially similar form for publication of the material as it may appear in the journal *Aging.* The dissertation author was the primary investigator and author of this paper. Co-authors were Max Shokhirev, Leo Andrade, Silvio Gutkind, Ramiro Iglesias-Bartolome, and Gerry Shadel.

CHAPTER 3 Unbiased, global mass spectrometry of conditioned medium (CM) and extracellular vesicles (EVs) in NOK senescence.

Mass spectrometry was performed on conditioned medium (CM) and proteins that were enriched for EVs from CM (2 replicates from each of Donors 1508 and 1415, 1 replicate from Donor 1408) at 3 time points (early, middle, and late). NOKs were cultured in defined medium without serum. As with the RNA-seq results, the first analysis of the mass spec results was performed from an unbiased perspective.

3.1 Ultracentrifugation enriches for EVs

The EV enrichment protocol uses differential centrifugation, filtering, and ultracentrifugation (UC), yet some non-vesicular proteins remain in the UC pellet. Prior to filtering, a sample of CM was set aside, and 10 µg of protein from that sample was analyzed, as was the entire UC pellet. Mass spectrometric analysis identified approximately 2,500 proteins that were present in at least one of the thirty (CM and EV for each of the 5 replicates at 3 time points) samples (Supp. File 3). Two known surface markers of exosomes, CD81 and CD151, were present in the UC pellet, although they were not plentiful enough to be found in the correlating CM samples, showing that the process effectively enriched for EVs (Fig. 3.1 and Supp. File 3). The UC product is hereafter referred to as “the EV pellet.”

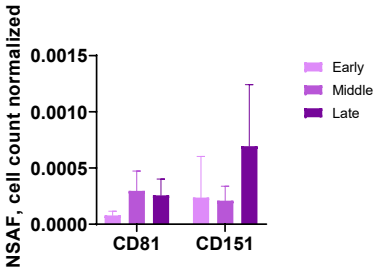

Figure 3.1. Enrichment for exosomal markers by UC of CM. Mass spectrometry results are expressed as NSAF per 10^6 cells (spectral abundance factor normalized for protein size and cell count).

3.2 Top upregulated and downregulated proteins in CM and EVs

Overrepresentation analysis of the CM and EV proteins revealed some overlap in the operative pathways for the proteins secreted in soluble versus vesicular form, but several differences as well. The analysis identified proteins with strong differential expression ($p < 0.01$) from both the early to late and mid to late passages (Supp. Files 4 & 5). None of the proteins were differentially expressed with this level of significance from early to mid passages. Protein folding was an important pathway for proteins released by both routes, as heat shock proteins and isomerases were increased with senescence in both the CM and EV fractions (Fig. 3.2). However, the top 2 functions for CM were regulation of membrane permeability and pyruvate metabolic process (Fig. 3.2), whereas the top 2 for EV were homotypic cell-cell adhesion and chromatin assembly or disassembly (Fig. 3.2).

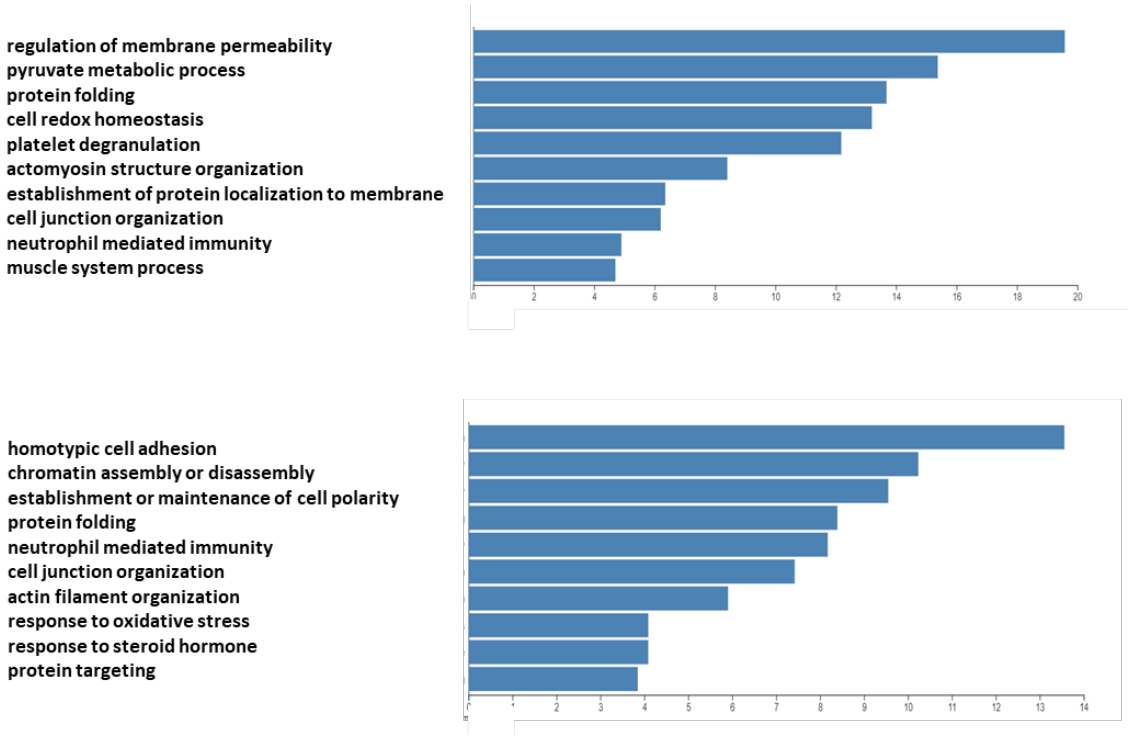

Figure 3.2. GO analysis of secreted proteins increased with senescence. CM (top) and EV pellet (bottom). Y-axes show enrichment ratio.

Mass spec results from CM and the EV pellet were also analyzed for significant ($p < 0.05$) changes, comparing each of the three stages (Supp. Files 4 and 5). The top five proteins for five of the six comparisons changed upward (Table 3.1A-3.1E). The exception was changes in the EV pellet from early stage to mid stage, for which two proteins, components of the 60S ribosomal subunit (L36a and L36a-like), declined significantly (Table 3.1F). As the ProLuCID software can attribute the same spectral counts to two proteins that contain the same peptides, and these two proteins are similar, only one of them may actually have changed significantly.

There was an overlap between proteins increasing from early to late and those increasing from mid to late (Table 3.1A-2.1D), suggesting an uninterrupted increase in secretion of these proteins as the percentage of senescent cells in the population grew. The most significantly (lowest adjusted p-value) changed proteins from early to late for CM and EVs were two members of the S100A family of calcium-binding proteins: S100A6 for CM and S100A2 for the EV pellet. S100A molecules are damage-associated molecular patterns (DAMPs) that promote inflammation (56). Another top increased protein in CM, HSP90, has previously been found in both vesicular and non-vesicular fractions (57) and is also a DAMP (22). Triosephosphate isomerase (TPI), an enzyme of glycolysis, may be ejected by NOKs to subvert reliance on the glycolytic metabolism employed by cancer cells to survive and proliferate (*i.e.,* the Warburg effect). Major vault protein accounts for the largest portion of the mass of vaults, which are cytoplasmic, non-vesicular ribonucleoprotein structures that can be released by cells (57). Ubiquitin-fold modifier 1 is a ubiquitin-like molecule. Its covalent addition to a protein may play a role in its being sorted into an EV (58). The only top five protein also present in the clean, negative control medium that was not used in culture is serotransferrin. Its increase in CM with passaging suggests that NOKs may take up less of it as they senesce.

Table 3.1. Changes in proteins secreted with senescence progression. Top 5 significantly changed ($p < 0.05$) proteins in CM and EV pellet when comparing early, middle, and late passages. Only 2 proteins were significantly changed in the EV pellet when comparing mid to early passages.

A. CM Late vs Early	**Gene**	**Name**	**Direction**
	S100A6	Protein S100-A6	Up
	HSP90AA2P	Heat shock protein HSP 90-alpha A2	Up
	TPI1	Triosephosphate isomerase	Up
	HSP90AB2P	Putative heat shock protein HSP 90-beta 2	Up
	SH3BGRL3	SH3 domain-binding glutamic acid-rich-like protein 3	Up
B. EV Late vs Early	**Gene**	**Name**	**Direction**
	S100A2	Protein S100-A2	Up
	MVP	Major vault protein	Up
	SERPINH1	Serpin H1	Up
	UBE2V2	Ubiquitin-conjugating enzyme E2 variant 2	Up
	GSN	Gelsolin	Up
C. CM Late vs Mid	**Gene**	**Name**	**Direction**
	TPI1	Triosephosphate isomerase	Up
	HSP90AA2P	Heat shock protein HSP 90-alpha A2	Up
	HSP90AB2P	Putative heat shock protein HSP 90-beta 2	Up
	S100A6	Protein S100-A6	Up
	SH3BGRL3	SH3 domain-binding glutamic acid-rich-like protein 3	Up
D. EV Late vs Mid	**Gene**	**Name**	**Direction**
	S100A2	Protein S100-A2	Up
	MVP	Major vault protein	Up
	GSN	Gelsolin	Up
	UFM1	Ubiquitin-fold modifier	Up
	SERPINH1	Serpin H1	Up
E. CM Mid vs Early	**Gene**	**Name**	**Direction**
	LGAL53BP	Galectin-3-binding protein	Up
	APP	Amyloid-beta precursor protein	Up
	IGFBP7	Insulin-like growth factor-binding protein 7	Up
	TF	Serotransferrin	Up
	AGRN	Agrin	Up
F. EV Mid vs Early	**Gene**	**Name**	**Direction**
	RPL36A	60S ribosomal protein L36a	Down
	RPL36AL	60S ribosomal protein L36a-like	Down

A critical application of profile results is their use to assess which aspects of *in vitro* senescent cells are most prevalent *in vivo* among individuals suffering from the pathologies of aging. A recent proteomic analysis of Alzheimer's disease (AD) brain and cerebrospinal fluid

(CSF) identified astrocyte/microglial metabolism proteins that were significantly increased in AD CSF of a cohort of patients compared to a control group (59). Five of the most significantly increased were also significantly up in the NOK EV pellet, comparing late to early passages: CD44, peroxiredoxin 1, lactate dehydrogenase (LDH) B-chain, pyruvate kinase, and GAPDH (Supp. File 5). The increases in LDH B-chain, pyruvate kinase, and GAPDH, as well as the increase in TPI in CM noted above, suggest that secretion of enzymes of glycolysis may be a biomarker of both senescence and AD. Indeed, other enzymes involved in glycolysis were significantly increased with senescence in NOK CM (LDH A, B, and C chains, fructose-bisphosphate aldolase A and C, phosphoglycerate mutase 2) or the EV pellet (LDH A chain, fructose bisphosphate aldolase A and C, and phosphoglycerate mutase 1) (Supp. Files 4 & 5).

3.3 Additional proteins of interest

The mass spec results show many other proteins whose secretion was significantly upregulated with senescence in NOKs (Supp. Files 4 & 5). Research indicates that some of them (*e.g.,* β-catenin and complement factor 3) could contribute to inflammation and diseases and dysfunctions of aging. Others (*e.g.,* peroxiredoxins) may provide insight into what is occurring inside NOKs as they senesce.

The connection between senescence and cancer, which has already been noted in the context of the RNA-seq results, is also evidenced in senescent NOK secretions. First, the amount of β-catenin in the EV pellet increased significantly with senescence (Supp. File 5). β-catenin is an element of canonical Wnt pathway signaling. When produced by a cell, β-catenin that is located in the cytosol translocates to the nucleus in response to binding of the Wnt ligand to its receptor, Frizzled, a transmembrane protein. In the nucleus, β-catenin associates with and positively regulates transcription factors for Wnt target genes. An excess of Wnt pathway signaling is associated with certain cancers (60) and stem cell dysfunction in skeletal muscle (61).

β-catenin can be released in EVs that are taken up by other cells, where it can translocate to the nucleus and induce Wnt pathway transcriptional activity (62). Second, another cancer-associated protein that was significantly increased with senescence, in this case in both the EV pellet and CM, was complement component 3 (C3) (Supp. Files 4 & 5). C3 contributes to innate immunity when it is cleaved; the C3b fragment opsonizes pathogens or apoptotic cells to attract immune cells and both C3a and C3b interact with receptors on immune cells (63). Among the cancers in which it has been found to be overexpressed and secreted is oral cancer (64).

Certain peroxiredoxins were significantly increased in CM and the EV pellet, comparing the late to early passages. Peroxiredoxins are antioxidant enzymes that reduce and detoxify hydrogen peroxide, lipid hydroperoxides, and peroxynitrite. After being oxidized, peroxiredoxins can be restored to their prior state by thioredoxins; however, they can also be inactivated if peroxide levels are particularly high (65). Peroxiredoxins 1 and 6 were significantly increased in CM (Supp. File 4) and peroxiredoxins 1 and 5 were significantly up in the EV pellet (Supp. File 5). Oxidized peroxiredoxin 1 has been found in exosomes released by certain cell types, which may be a way to clear non-functional proteins from the cell (66). Conceivably, transgenic overexpression of peroxiredoxins could delay senescence.

With the exception of Section 3.3, Chapter 3 has been submitted in substantially similar form for publication of the material as it may appear in the journal *Aging.* The dissertation author was the primary investigator and author of this paper. Co-authors were Max Shokhirev, Leo Andrade, Silvio Gutkind, Ramiro Iglesias-Bartolome, and Gerry Shadel.

CHAPTER 4 Inflammatory pathways are upregulated in NOK senescence.

Certain inflammatory aspects of senescence are known to operate in a range of cells. Different cell types, however, show variation in the degree to which they display these characteristics. NOKs exhibit some, but not all, of the features of these inflammatory pathways. Understanding the differences between cell types is necessary for the development of targeted therapeutics.

4.1 The canonical senescence associated secretory phenotype

The senescence associated secretory phenotype (SASP) encompasses inflammatory components, factors involved in transmitting senescence to other cells and altering the environment in a manner that facilitates tumorigenesis, and regulators of these elements. The most comprehensive single published list of these components catalogued approximately 70 proteins (19).

The RNA-seq data showed a strong ($p < 0.05$ and log2 fold increase > 1.5) increase in mRNA for 23 SASP components, while 3 components were similarly decreased, and 4 were not present (Fig. 4.1.1). The increases in mRNA were found in all SASP categories, including inflammatory factors, growth factors and their regulators, proteases, and protease inhibitors (Fig. 4.1.1). Increases for five SASP components were confirmed with RT-qPCR (Fig. 4.1.2). Comparison of mRNA levels at passages 5, 10, and final for eight major inflammatory SASP elements shows significant upregulation (Fig.4.1.3).

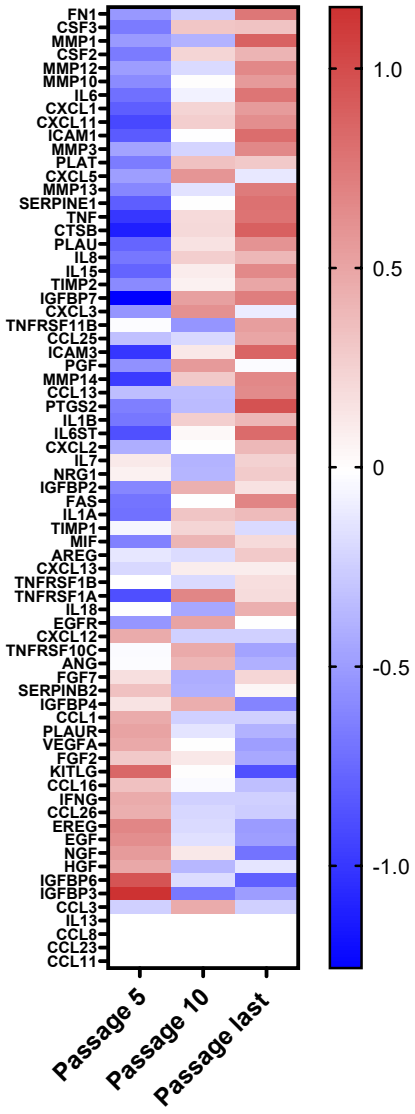

Figure 4.1.1. Heat map of SASP protein components. Z-scores of changes in mRNA show upregulation, downregulation, or little change. Completely white rows represent zero FPKM at all passages for all donors.

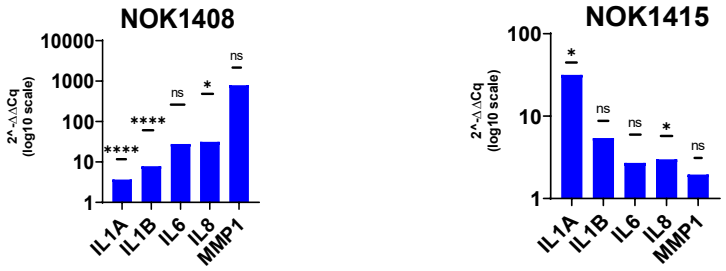

Figure 4.1.2. RT-qPCR results for selected SASP elements. Y-axis is $2^{-\Delta\Delta Cq}$ on a log10 scale. Passage 5 and last passage were normalized to GAPDH (ΔCq) and the last passage was then normalized to passage 5 (ΔΔCq). (Left, two replicates from Donor 1408; right, two replicates from Donor 1415.) Large difference between female (1408) and male donor (1415) for MMP1 is also seen in RNA-seq data. Y-axis scales differ. (Significance determined comparing last passage to passage 5, after normalization to GAPDH, using two-tailed t-test.) *p<0.05, **p<0.01, ***p<0.001, ****p<0.0001.

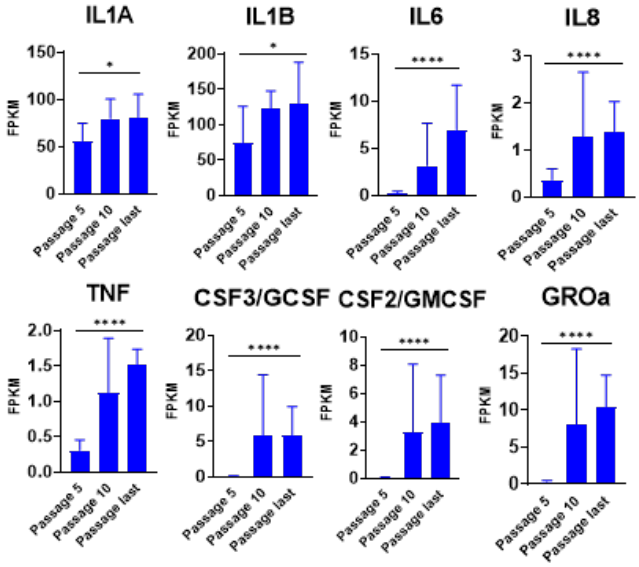

Figure 4.1.3. mRNA levels of 8 major inflammatory SASP elements. Increases from passage 5 to last passage were significant ($p < 0.05$) (Mean +SD). Y-axis scales differ. *p<0.05, **p<0.01, ***p<0.001, ****p<0.0001.

Analysis of proteins in CM shows functionality of the secretory aspect of the SASP in NOKs. A multiplex immunoassay found significant increases in the same eight selected major inflammatory factors (Fig. 4.1.4). Notably, IL-1α, which is both an inducer and target of NF-κB

transcription, was secreted by NOKs in increasing amounts as cells senesced, although the quantity varied between samples (from 74.68 to 1888.2553 pg/ml/10^6 cells at the final passage). IL-1α is displayed on the surface of senescent fibroblasts, but little is secreted by those cells (67), providing another example of a difference between NOKs and fibroblasts. Other SASP proteins were present in CM in increasing amounts, despite the fact that changes in their mRNA levels were not significant (other than IL-15) (Fig. 4.1.5). Except for VEGFA, the amounts were small. Secretion of EGF increased with senescence, despite the significant decrease in mRNA.

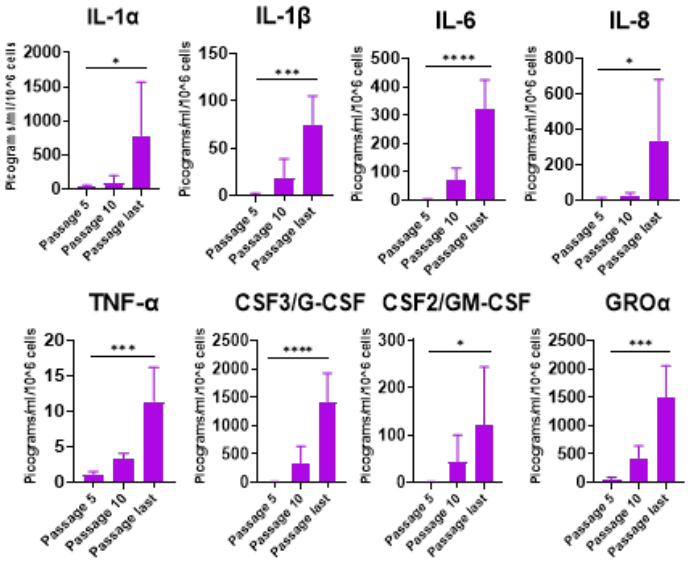

Figure 4.1.4. Protein levels of 8 major inflammatory SASP elements in CM. Multiplex immunoassay results (Mean ±SD). Results normalized by cell count and by subtracting amounts of these proteins contained in the same quantity of clean medium. Y-axis scales differ. (Significance determined by t-tests.) *p<0.05, **p<0.01, ***p<0.001, ****p<0.0001.

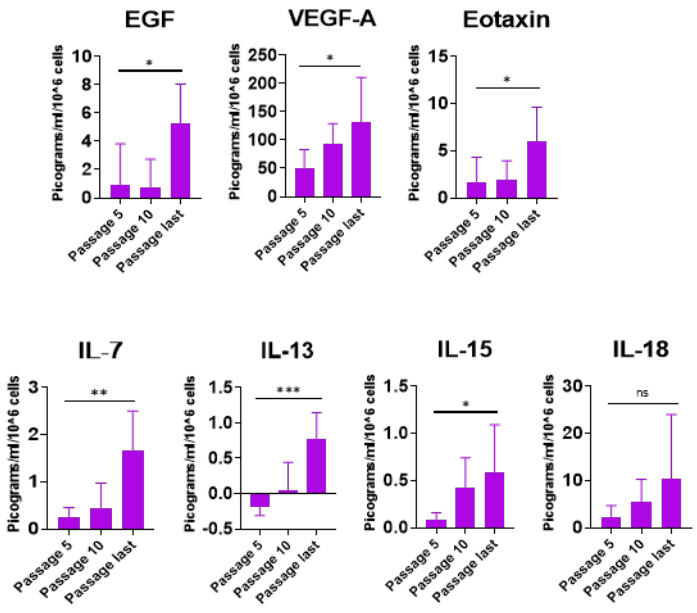

Figure 4.1.5. Protein levels of other SASP elements in CM. Determined and normalized as in Fig. 4.1.4. (Mean ±SD.) Y-axis scales differ. (Significance determined by t-test.) *p<0.05, **p<0.01, ***p<0.001, and ****p<0.0001.

Proteomic analysis found that five SASP components increased significantly ($p < 0.05$) in the EV pellet with senescence: SERPINE1, cathepsin B, IL-18, TIMP1, and EGFR (Supp. File 5). Notably, IL-18 mRNA did not significantly change (Supp. File 1). This suggests that EVs may play a greater role in perpetrating chronic inflammation via the SASP than has been appreciated previously.

4.2 The NF-κB, interferon, and p38MAPK pathways

Three major inflammatory pathways have been found to be upregulated in most forms of cellular senescence: NF-κB, cGAS-STING (cyclic GMP-AMP synthase and stimulator of interferon genes), and p38MAPK. Initially, NF-κB is activated as part of the DNA damage response (68). Nuclear or mitochondrial DNA (mtDNA) in the cytosol is detected by cGAS; this triggers the STING pathway, which activates the IFN and NF-κB signaling pathways (32, 43). Activation of p38MAPK in senescent cells has also been found to increase NF-κB transcriptional

activity (69). The RNA-seq results showed strong upregulation of many elements of the NF-κB pathway (Fig. 4.2.1). Upregulated genes include activators of NF-κB (*e.g., TLR3* and *TLR4*) and NF-κB target genes that either are (*e.g., CTSB, IL6*) or are not (*e.g., APOE, C3*) SASP components. Transcription of a few genes (*e.g., CXCL3, CXCL5*) rose in the early stages, and then declined. This might suggest a partially successful effort to dampen the inflammatory cycle. Immunoblotting confirmed the presence of transcriptionally active phosphorylated p65 from passage 5 to the last passage (Fig. 4.2.1). IFN pathways were also upregulated at the mRNA level (Fig. 4.2.2). This occurred despite the fact that mRNA FPKM measurement was zero or fractional for IFN-γ, IFN-β, and 13 subtypes of IFN-α, for nearly all samples (Supp. File 1), and the highest concentration of secreted IFNs measured was in the low single-digits of picograms per milliliter (Fig. 4.2.2). This is less than 0.1% of the amount used to induce transcription of IFN pathway genes in cell culture (70). Upregulation of IFN signaling pathways despite a lack of IFNs is a phenomenon previously observed in cellular senescence as a consequence of chromatin release into the cytoplasm (43), and in response to chronic mtDNA-mediated cGAS-STING signaling (71). It likely denotes either a cell-intrinsic, IFN-independent mechanism or an adaptation to chronic, low-level IFN signaling. Among the genes upregulated were a promoter of apoptosis (*XAF1*), and a number of IFN-induced genes (*e.g., CXCL10, IFI6, IFIT1, IFIT2, IFIT3, ISG15, OAS2*). A few IFN pathway genes (*e.g., EGR1, GBP2, NUP210*) were downregulated (Fig. 4.2.2). Downregulation of *EGR1*, a transcription factor for a suppressor of cytokine signaling, is consistent with upregulation of IFN-like signaling. One of the four p38MAPK genes, *MAPK11*, was significantly increased, and an inhibitor, *CHP2*, was significantly decreased (Fig. 4.2.3). The pattern of dominance in upregulation of inflammatory signaling that is seen with the NF-κB and IFN pathways is, however, absent.

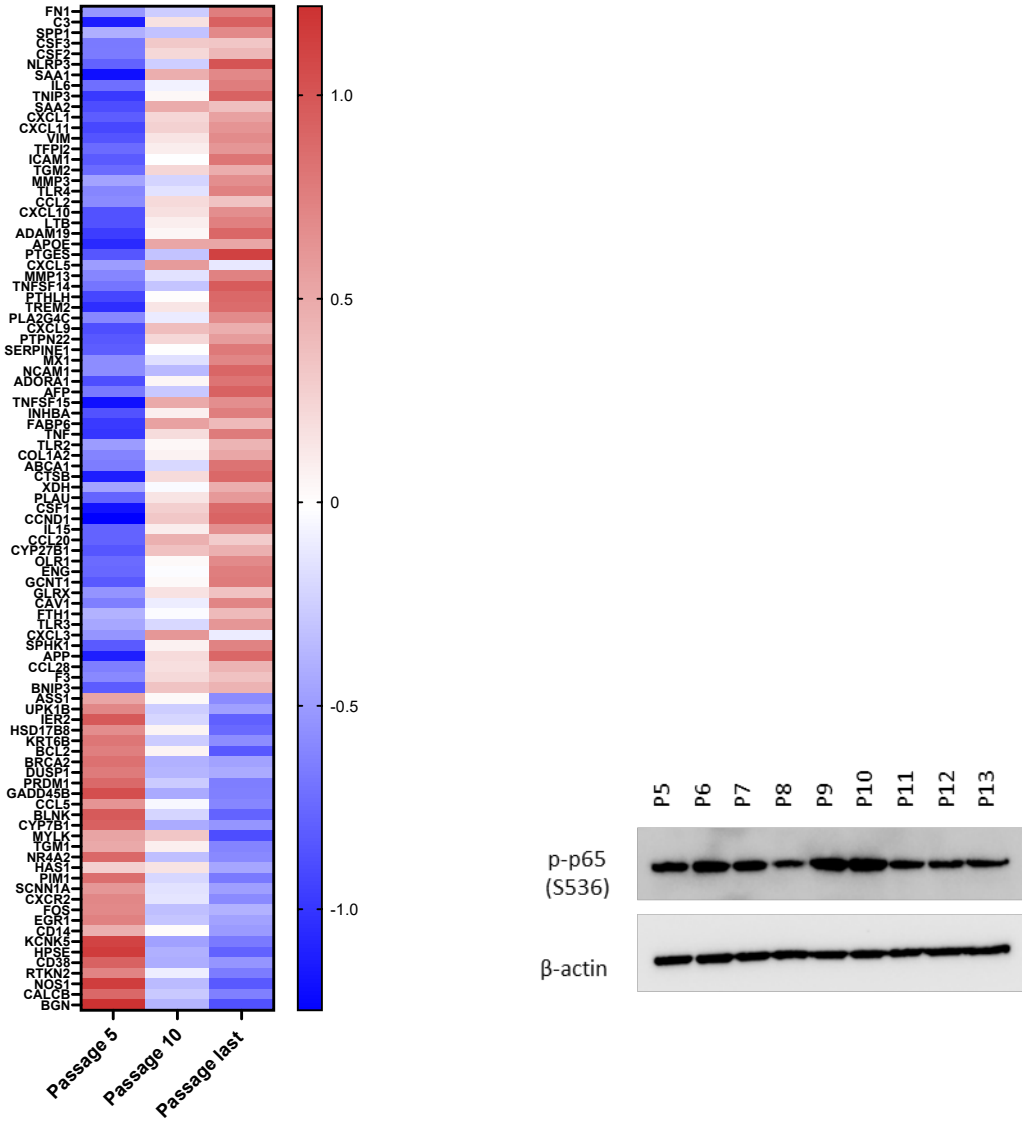

Figure 4.2.1. NF-κB pathways activation. Left, heat map of differentially expressed genes (DEGs) in NF-κB pathways. Z-scores of mRNA changes show a greater number of upregulated genes compared to those downregulated. DEGs defined as adjusted p-value of change from passage 5 to last passage was < 0.05 and log2-fold change >1.5 or less than -1.5. Right, immunoblot for p-p65 (S536), an indication of transcriptionally active NF-κB (Donor 1415).

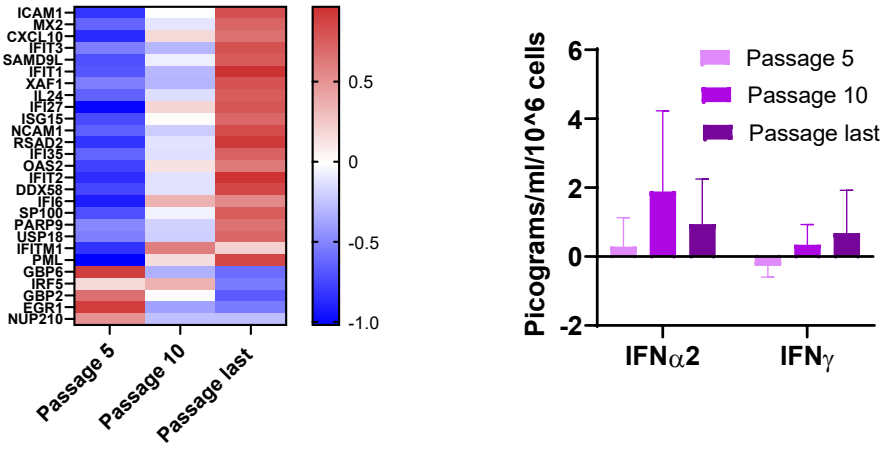

Figure 4.2.2. IFN pathways activation. Left, heat map of DEGs in IFN pathways. Z-scores of mRNA changes. DEGs defined as in Fig. 4.2.1. Right, IFN levels in CM are low at all stages. Determined and normalized as in Fig. 4.2.1. None of the changes in IFNs were significant ($p < 0.05$).

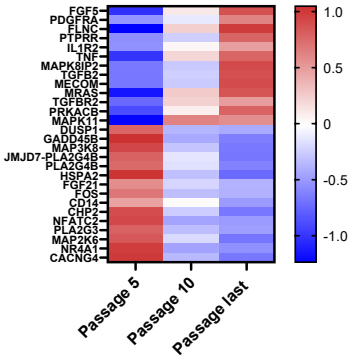

Figure 4.2.3. p38MAPK pathways activation. Heat map of DEGs in p38MAPK pathways. Z-scores of mRNA changes. DEGs defined as in Fig. 4.2.1.

One subset of IFN pathway genes, the IFN-related DNA damage resistance signature (IRDS) genes, is noteworthy. This group of 49 IRDS genes has been identified as a "survival signature" found in cancer cells that are resistant to death induced by DNA-damaging therapies (72). The mRNA for 24 of these IRDS genes was differentially expressed in NOKs with senescence, with a strong trend of upregulation (Fig. 4.2.4). This suggests that these genes could be productively targeted by senolytic therapies that could also be used in cancer treatments.

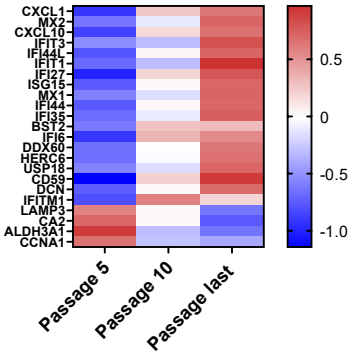

Figure 4.2.4. IRDS DEGs. Heat map shows z-scores of mRNA changes in IFN pro-survival gene set. DEGs defined as in Fig. 4.2.1.

4.3 The NLRP3 inflammasome

The NLRP3 inflammasome, when assembled, activates caspase 1, which cleaves pro-IL-1β and pro-IL-18, after which they are released from the cell (73). Transcription of genes for IL-1β and NLRP3 (both NF-κB targets) significantly increased with senescence (Supp. File 1), the amount of IL-1β in CM increased with senescence (Fig. 4.1.4), and the amount of IL-18 (another NF-κB target) in the EV pellet increased with senescence (Supp. File 5). The NLRP3 inflammasome adaptor protein ASC (PYCARD), was found in the EV pellet, increasing with senescence (Supp. File 5). Thus, senescing NOKs may form inflammasomes that induce secretion of the inflammatory cytokine IL-18 in EVs (74). In this regard, significant ($p < 0.05$) increases in amyloid-β precursor protein were found in the proteomic analysis of both CM and the EV pellet (Supp. Files 4 & 5); amyloid-β is known to activate the NLRP3 inflammasome (75). Formation of inflammasomes during senescence adds another layer of inflammation to the NOK SASP.

Chapter 4 has been submitted in substantially similar form for publication of the material as it may appear in the journal *Aging.* The dissertation author was the primary investigator and author of this paper. Co-authors were Max Shokhirev, Leo Andrade, Silvio Gutkind, Ramiro Iglesias-Bartolome, and Gerry Shadel.

CHAPTER 5 Immune evasion elements are upregulated in NOK senescence.

Despite the detriment to the organism, senescent cells are known to engage mechanisms that make their destruction more difficult. Judging by the RNA-seq results, a number of death-avoidance mechanisms appear to be upregulated in NOKs as they senesce. Both senolytic and anti-cancer treatments are being developed based on approaches for defeating such mechanisms.

5.1 Anti-apoptosis genes

The B cell lymphoma 2 (Bcl-2) family includes both pro- and anti-apoptotic members. Residing in the mitochondrial membrane, the Bcl2 proteins that inhibit apoptosis (Bcl-2, Bcl-2L1, Bcl-2L2, Bcl-2L3, Bcl-2L10, and Bcl-2A1) do so by preventing opening of the mitochondrial permeability transition pore and the consequent release of apoptogenic proteins from mitochondria (76). Some senolytic drugs work by inhibiting anti-apoptotic Bcl-2 elements when they are upregulated in senescence (77).

NOK senescence had differing effects on mRNA levels of anti-apoptotic members of the Bcl2 family (Fig. 5.1 & Supp. File 1). RNA-seq analysis showed that *BCL2, BCL2L2* (also called *BCL-W,* and one of the genes upregulated in the core signature of senescence discussed in Chapter 2, above), and *BCL2L10* (also called *BCL-B*) declined significantly with senescence. The changes in *BCL2L1 (als*o referred to as *BCL-XL*) and *BCL2L3* (also called *MCL1*) were not significant. In contrast, levels of mRNA for *BCL2A1* (also called *BFL1*), a target of NF-κB transcription that is overexpressed in some types of cancers (78), increased significantly, indicating that the protein for which it codes, Bcl-2-related protein A1, may be a possible senolytic target (79).

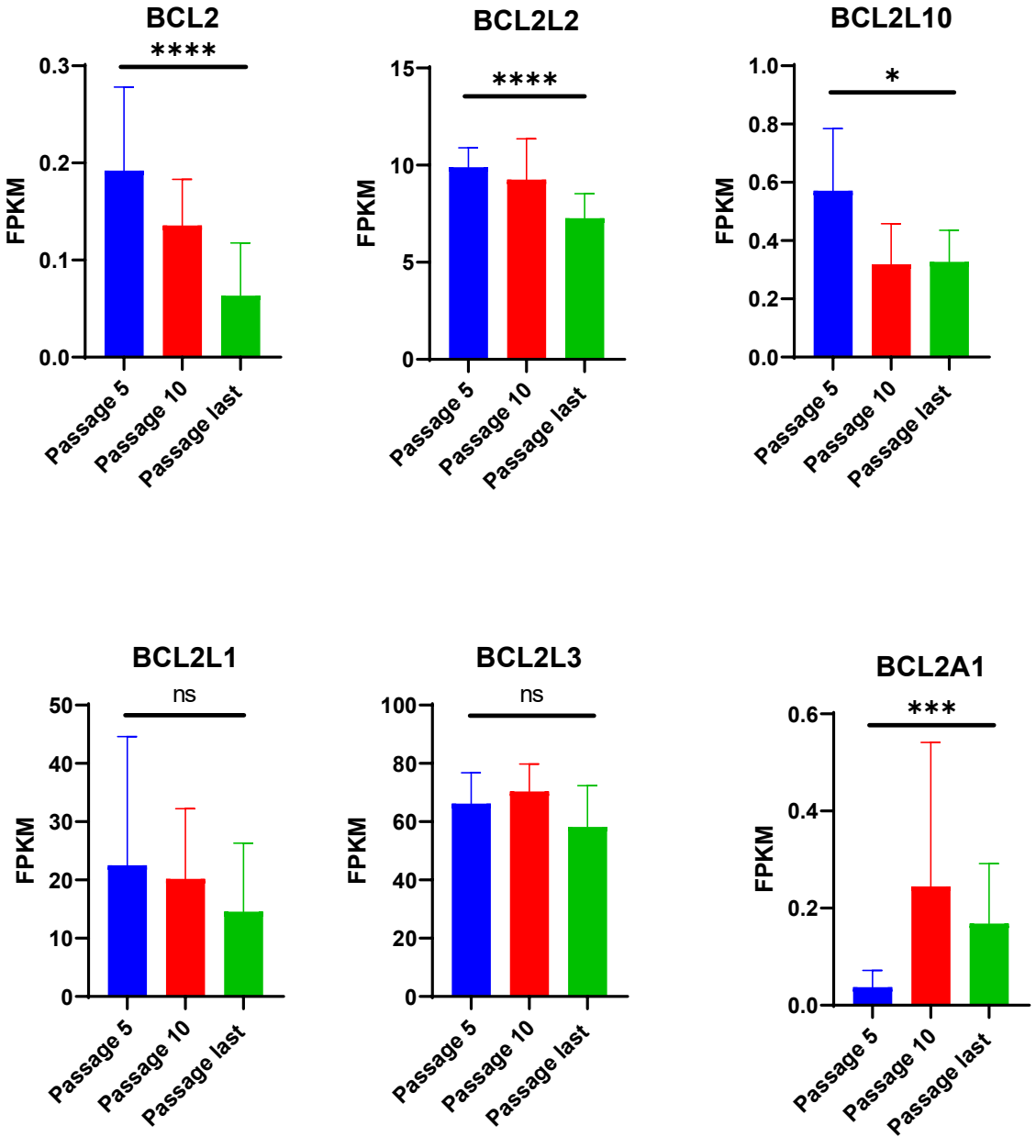

Figure 5.1. mRNA expression of anti-apoptotic Bcl-2 family members. (Y-axis scales differ.) *p<0.05, **p<0.01, ***p<0.001, ****p<0.0001.

5.2 Human leukocyte antigens (HLAs)

Classical HLAs (HLA-A, HLA-B, and HLA-C) are cell surface molecules that serve critical functions by virtue of their interactions with cells of the immune system. They present antigen to T cells. They also induce inhibition when they bind receptors on natural killer (NK) cells. Both CD8+ T cells and NK cells are cytotoxic and can kill senescent cells (13, 80), using perforin to create pores in the target cells, through which granzyme proteases are released into the target. Whether an NK cell destroys a target cell can depend on the balance of inhibitory and activating signals it receives from the cell. (Indeed, one such activating surface molecule known to be upregulated in some senescent cells, ULBP2 (80), was significantly increased at the mRNA level in senescing NOKs. (Supp. File 1)). Whether a CD8+ T cell destroys a target cell can depend on whether an antigen bound to an HLA molecule on the cell is recognized by the T cell as a non-self peptide. An antigen can be identified by a T cell as non-self, leading to destruction of the cell presenting it, if it is produced by a pathogen or if it is generated by the body but is sufficiently mutated that it is seen as non-self (such as a neoantigen produced by a cancer cell).

In NOKs, transcription of the genes for the classical HLA molecules shows a divergent pattern, similar to the DNA repair genes discussed in Chapter 2, above. There was upregulation at the mRNA level, with NOK senescence, of these three HLA genes for the two female donors (Donors 1408 and 1508), but a declining trend for the male donor (NOK1415) (Fig. 5.2.1 & Supp. File 1). These changes were significant ($p < 0.05$) only for HLA-A and B (Supp. File 1). If classical HLA molecules are displayed on the NOK surface, the result could be evasion of NK cell killing due to binding of the HLAs to inhibitory receptors on the NK cell. At the same time, depending on whether the antigen peptide bound by the HLA molecule is seen as self or not, it could either inhibit or enable destruction of the senescent cell by CD8+ T cells. If the peptide is sufficiently mutated (*e.g.,* as a consequence of the downregulation of DNA repair mechanisms described above), it may provoke an immune reaction. Chains from these 3 HLA proteins were also found

in the EV pellet (Supp. Files 4 & 5), indicating that they are released by NOKs (81), and thus may serve as decoys for NK or CD8+ T cells.

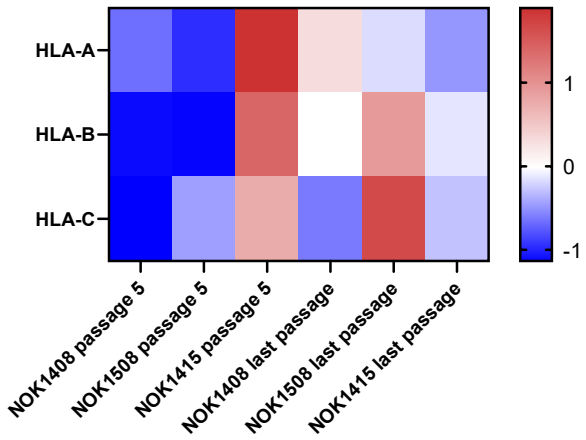

Figure 5.2.1. Heat map of Z-scores for classical HLA molecules.

A similar pattern was observed in the mRNA for two non-classical HLAs, HLA-E and HLA-F, and one gene whose classification as a pseudogene is being reconsidered (82), HLA-H (Fig. 5.2.2 & Supp. File 1), although only the change for HLA-H was significant (Supp. File 1). The functions of these proteins are less understood. However, upregulation of HLA-E has been found to allow senescent cells to evade destruction by both NK cells and CD8+ T cells (13).

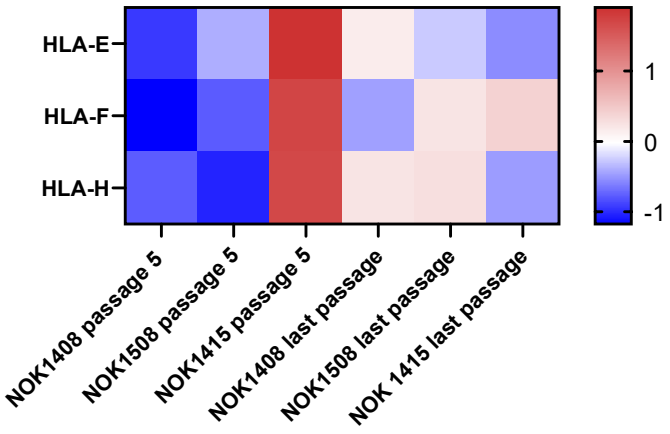

Figure 5.2.2. Heat map of Z-scores for non-classical HLA molecules.

5.3 Decoy receptors

In addition to killing their targets using perforin and granzymes, NK and CD8+ T cells can induce apoptosis via binding of their cell-surface Fas ligand (FasL) to Fas receptors on the target. The RNA-seq results showed significant upregulation with senescence of mRNA for the decoy receptor TNFRSF6B, which binds FasL (Fig. 5.3.1 and Supp. File 1). The Fas decoy receptor has two versions: the first is soluble (83), and the second is membrane-bound, but lacks the cytoplasmic death domain necessary for transmitting the apoptotic signal (84). TNFRSF6B was present in some of the mass spec samples, both CM and EVs (Supp. File 3).

Another decoy receptor, TNFRSF10D, binds TNF-related apoptosis-inducing ligand (TRAIL), which is produced by NK and CD8+ T cells. Binding of TRAIL normally causes cell death, but TNFRSF10D, like membrane-bound TNFRSF6B, lacks a death domain and cannot effectuate that result (85). mRNA for TNFRSF10D exhibited the divergent pattern seen with HLA molecules (Fig. 5.3.2 and Supp. File 1).

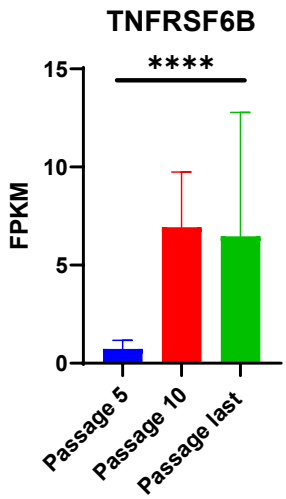

Figure 5.3.1. mRNA expression for TNFRSF6B decoy receptor. *p<0.05, **p<0.01, ***p<0.001, ****p<0.0001.

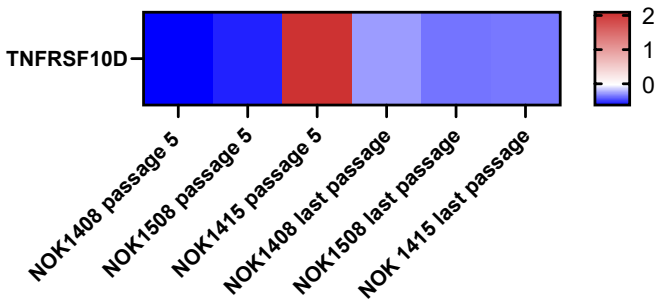

Figure 5.3.2. Heat map of Z-scores for TNFRSF10D.

5.4 Other immune suppressive molecules

Two additional immune suppressive molecules, CD73 and CD113, were also upregulated at the mRNA level. Each of these proteins has been found to suppress the immune system and cancer biologists have been researching ways to inhibit them, so that immune cells are not prevented from performing their normal functions (86, 87). As with inhibitors of anti-apoptotic members of the Bcl-2 family, this may present an opportunity for application of cancer drugs to facilitating destruction of senescent cells.

CD73, encoded by the *NT5E* (ecto-5′-nucleotidase) gene, is a plasma membrane protein that catalyzes the hydrolysis of extracellular nucleotides. CD73 acts as an immune suppressor, because it generates free adenosine by hydrolysis of AMP, and this adenosine binds receptors on T and NK cells, bringing about cAMP-mediated blocking of their effector functions. CD73 is overexpressed in some cancers, and blocking antibodies are being evaluated as a treatment (88). mRNA for CD73 was significantly upregulated in senescent NOKs (Fig. 5.4 & Supp. File 1).

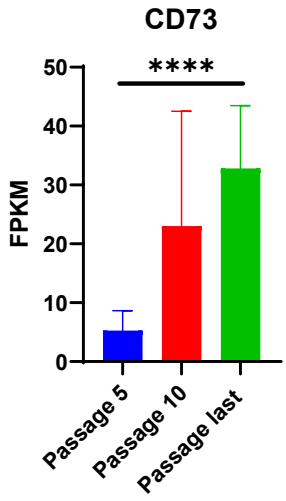

Figure 5.4.1. mRNA expression of CD73. *p<0.05, **p<0.01, ***p<0.001, ****p<0.0001.

CD113 (also called Nectin 3) is a ligand for the inhibitory receptor TIGIT (T cell immunoreceptor with Ig and ITIM domains). TIGIT is expressed on both NK and T cells. One example of the inhibitory effect of binding of TIGIT is that it has been shown to limit secretion of IFNγ by NK cells and CD8+ T cells (86). mRNA for CD113 was significantly upregulated in senescent NOKs (Fig. 5.5 & Supp. File 1).

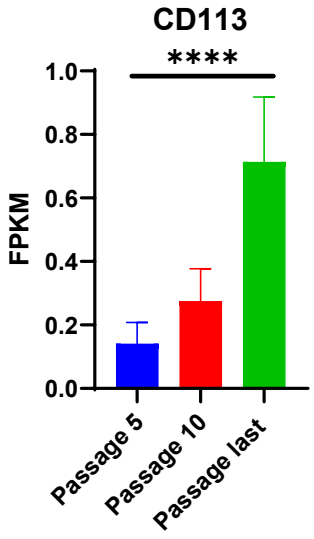

Figure 5.4.2. mRNA expression of CD113. *p<0.05, **p<0.01, ***p<0.001, ****p<0.0001.

Why do senescent cells engage in such contradictory activities? They upregulate genes for both pro- and anti-apoptotic molecules, and they secrete molecules designed to attract the immune system while simultaneously erecting defenses against it. In the context of cancer, it has been suggested that cells are essentially "selfish" and are sometimes able to circumvent the cooperative system that makes multicellular organisms possible (89). This ability to survive and proliferate would have been an advantage in a world of single-cell organisms. A senescent cell may be thought of as one that similarly attempts to avoid the body's enforcement of cooperation, but is only partly successful (*i.e.,* it survives, but does not replicate).

Chapter 6 New proposed SASP components upregulated in NOK senescence.

An important motivation to this work was to identify unacknowledged aspects of senescence that are evidenced more strongly in epithelial cells relative to fibroblasts, or that may be unique to epithelial cells. Based on the mass spectrometry results, addition of the following proteins to a more epithelial-inclusive SASP is hereby proposed: heat shock protein 60 (HSP60), S100A2, S100A6, S100A9, and S100A11. These were selected for two reasons. First, these proteins were found, in quantities that were significantly higher at late passages than early, in the EV pellet or both the EV pellet and CM (Fig. 6.1). Second, each of these proteins is an endogenous ligand for one of two pro-inflammatory pattern-recognition receptors: the receptor for advanced glycation end products (RAGE) and Toll-like receptor 4 (TLR4) (90-92). At the mRNA level, only S100A2 and S100A6 significantly increased, and HSP60 mRNA declined significantly with senescence (Fig. 6.2).

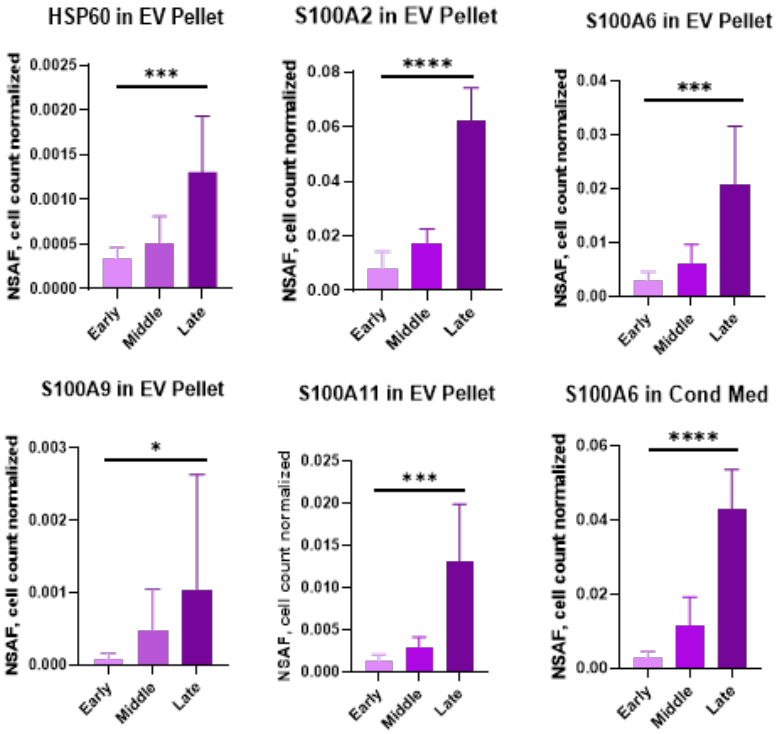

Figure 6.1. Mass spectrometry analysis of proposed SASP additions. Selected proteins significantly increased in EV pellet or CM (Mean ±SD). Y-axis scales differ. *p<0.05, **p<0.01, ***p<0.001, **** p<0.0001.

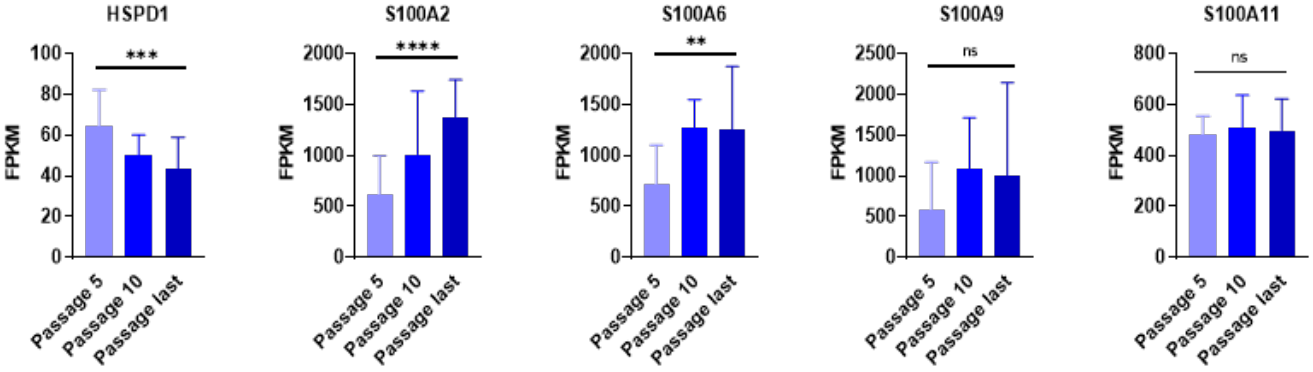

Figure 6.2. mRNA levels of proposed SASP additions. (Mean ±SD). Y-axis scales differ. *p<0.05, **p<0.01, ***p<0.001, **** p<0.0001.

HSP60, one of these nominated proteins, primarily localizes to mitochondria. It has, however, been found in association with the outer surface of the plasma membrane of certain cancer cells and cardiomyocytes, and the membrane of EVs secreted by these cells (91, 92). IF consistently showed EVs staining positive for HSP60 outside the NOK cell boundary (Fig. 6.3). Transmission electron microscopy (TEM) and immunogold labeling of EVs enriched from NOK CM was employed to determine whether HSP60 was on the surface of these EVs. TEM showed EVs that labeled positive for surface HSP60 (Fig. 6.4), indicating that EV-associated HSP60 is available to interact with receptors on target cells.

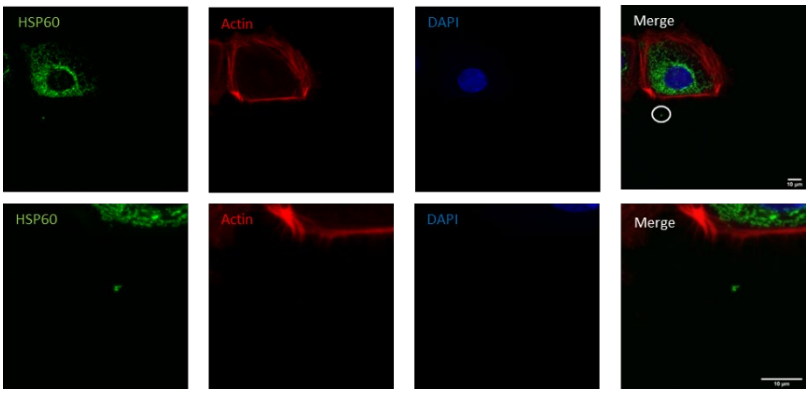

Figure 6.3. IF staining of NOKs for HSP60 and actin. Representative example of many small bodies observed that were positive for HSP60 and outside cell boundary. (Top row, 63x objective and zoom = 1; bottom row, same cell and EV, 63x objective and zoom = 3).

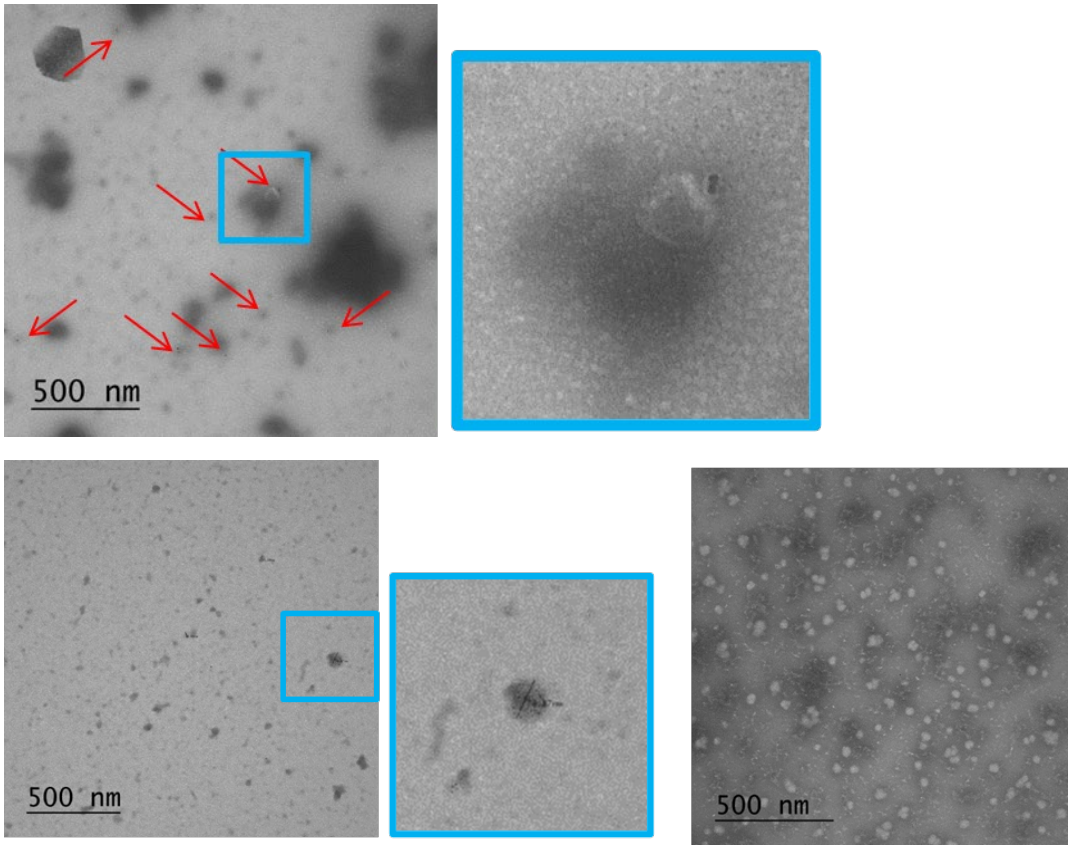

Figure 6.4. TEM of vesicles from EV pellet. Labeling for surface HSP60 (top left, and 4x enlargement, top right). Positive control exosomal marker CD81 (bottom left, and 3x enlargement center). Negative control (secondary antibody and beads, no primary antibody) shows no labeling of vesicles (bottom right). (Images by Leo Andrade.)

These five additions to the SASP are proposed in recognition of their potential contribution to chronic inflammation in senescence. One of the nominated proteins, HSP60, is appended to the membrane of EVs released by senescing NOKs. Such an event by senescing cells has been the subject of some speculation (93), but has not previously been shown. Moreover, TLR4, which is bound by HSP60, was significantly upregulated at the mRNA level as NOKs senesce (Supp. Table 1), suggesting a mode for transmitting or reinforcing senescence in a paracrine manner between NOKs by activation of NF-κB.

Chapter 6 has been submitted in substantially similar form for publication of the material as it may appear in the journal *Aging.* The dissertation author was the primary investigator and author of this paper. Co-authors were Max Shokhirev, Leo Andrade, Silvio Gutkind, Ramiro Iglesias-Bartolome, and Gerry Shadel.

Chapter 7 EVs from senescent NOKs activate interferon pathway signaling in THP-1 monocytes.

The contribution of the senescent NOK secretome to the inflammatory milieu depends in large part on its effects on other cells. Having characterized components of the NOK EV SASP, the question arose as to what effect EVs isolated from the secretions of senescent NOKs might have on inflammatory pathways in a cell of the immune system.

THP-1 monocytes with an IFN reporter system were used to address this question. These cells secrete luciferase transcribed from a gene under the control of an ISG54 minimal promoter in conjunction with five ISREs. EVs from late passage CM were isolated by size exclusion chromatography. An EV fraction whose size was consistent with exosomes and small microvesicles was used (Fig. 7.1). These EVs were incubated with the THP-1 cells, either with or without the STING inhibitor H-151 (94), to address the possible role of DNA-mediated IFN signaling. Vehicle-treated THP-1 cells and cells treated with the DNA analog poly(dA:dT) in complex with a cationic lipid transfection reagent to facilitate entry into the cells served as controls. Effectiveness of STING inhibition by H-151 was demonstrated by the steep reduction in transcription from the IFN pathway binding sites when H-151 was added to poly(dA:dT)-treated cells (Fig. 7.2).

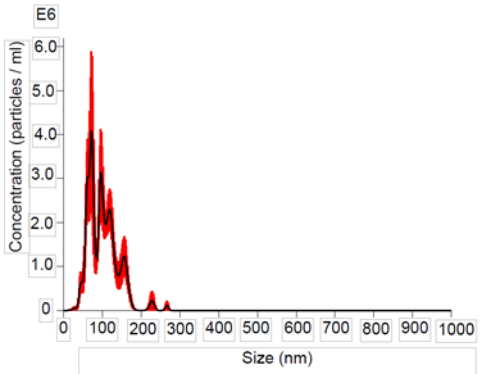

Figure 7.1. NanoSight analysis of EVs isolated by SEC. Graph shows vesicle size and quantity. (Error bars indicate +/-1 standard error of the mean.)

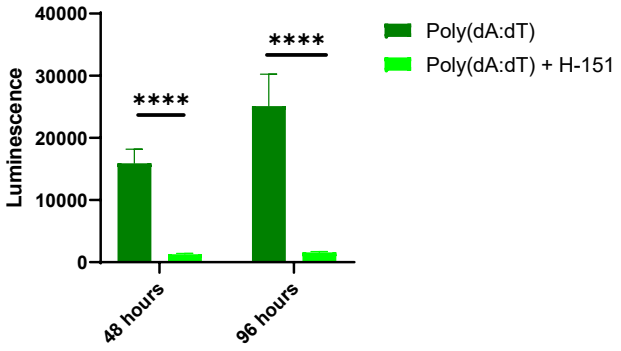

Figure 7.2. IFN transcription in THP-1 cells treated with poly (dA:dT). Over 96 hours, level of luciferase was strongly reduced by the addition of the STING inhibitor H-151. *p<0.05, **p<0.01, ***p<0.001, ****p<0.0001.

THP-1 cells showed an increase in transcription from the IFN reporter when incubated with EVs from senescent NOKs, which was sharply reduced by the addition of H-151 (Fig. 7.3). Given that cGAS-cGAMP-STING signaling is activated by cytosolic DNA, this suggested that the increase in IFN pathway signaling caused by EVs is mediated in large part by nuclear DNA, mtDNA, or both. Accordingly, DNA was isolated from the same batch of EVs used for the THP-1 experiment, in order to verify its presence and ascertain its nature. DNA from all human chromosomes and mitochondria was detected, with relatively even coverage for the autosomal chromosomes (average of 87 reads per kilobase for chromosomes 1-22) and coverage across mtDNA that was > 35-fold enriched compared to nuclear DNA, at 3,079 reads per kilobase (Supp. Table 6, Fig. 7.4). The presence of mtDNA in EVs was confirmed using droplet digital PCR, which allows for absolute quantification of target DNA copies (Fig. 7.4).

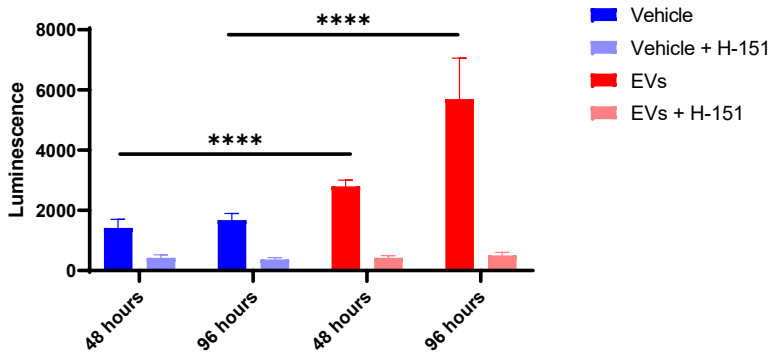

Figure 7.3. IFN transcription in THP-1 cells treated with EVs. Over 96 hours, level of luciferase was significantly higher for cells co-incubated with EVs from senescent NOKs compared to vehicle-treated cells, and was significantly reduced by the addition of the STING inhibitor H-151. Results for Fig. 7.2 & 7.3 show mean of 8 replicates for each condition ±SD. Readings in Fig. 7.2 & 7.3 were normalized by subtracting mean luminescence of wells containing only Quanti-Luc reagent. *p<0.05, **p<0.01, ***p<0.001, ****p<0.0001.

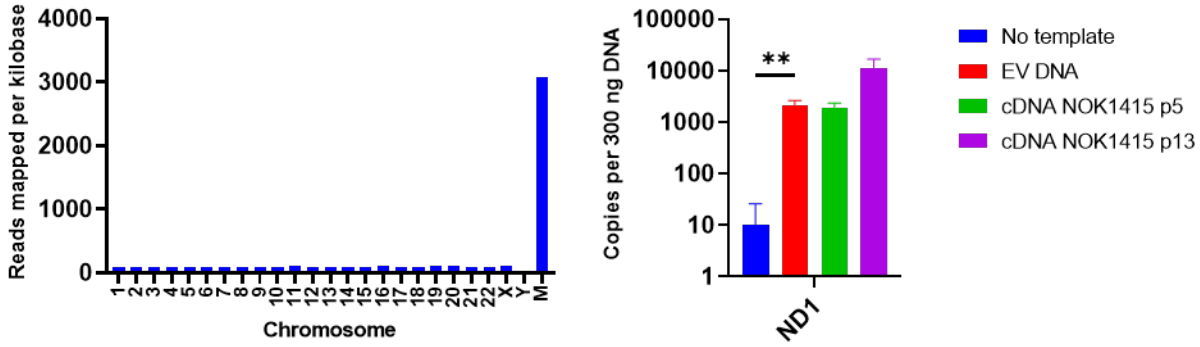

Figure 7.4. DNA is associated with EVs from senescent NOKs. Left, DNA sequencing. Right, ddPCR results for *MT-ND1* DNA. Fig. 7.2, 7.3 & 7.4 significance levels determined using t-test. For ddPCR, no template reaction was negative control and cDNA from whole cell RNA was positive control. For Fig. 7.2, 7.3 & 7.4, *p<0.05, **p<0.01, ***p<0.001, ****p<0.0001.

These data demonstrate that the vesicular components of the NOK SASP can induce inflammatory signaling in at least one type of immune cell and that part of this inflammation is likely due to DNA carried by the vesicles. It is also possible that interaction with EVs triggers signaling events that lead to cytoplasmic release of nuclear or mitochondrial DNA in the affected

cells. Vesicular secretion of large amounts of extracellular mtDNA has been found in studies of cancer cell lines (95), but less often in senescence research (96). It has been suggested that the generation of vesicles derived from mitochondria is instigated by oxidative damage (97). As yet unknown is whether specific portions of the mitochondrial genome are more likely to be released from the mitochondria and packaged into vesicles. Even if the entire mitochondrial genome is released, some sequences may be more prone to DNA damage that makes it difficult to map the fragments to the standard human mitochondrial genome sequence. EVs can be internalized by target cells by one of many possible interactions (*e.g.,* integrins and tetraspanins on the surface of the EVs associating with adhesion molecules on the surface of the target cells) (30). We anticipate that continued active investigation of the generation, content, and impact of EVs will yield further insights into how to ameliorate senescence.

Chapter 7 has been submitted in substantially similar form for publication of the material as it may appear in the journal *Aging.* The dissertation author was the primary investigator and author of this paper. Co-authors were Max Shokhirev, Leo Andrade, Silvio Gutkind, Ramiro Iglesias-Bartolome, and Gerry Shadel.

Chapter 8 Mitochondrial changes with NOK senescence.

Mitochondria play important and multifarious roles in aging, many of which are not yet well understood (98). They are, for example, the primary source of reactive oxygen species that damage macromolecules, such as DNA and proteins, a fact that led to the free radical theory of aging. At the same time, mitochondria can serve as an early warning system that transmits danger signals to the nucleus, resulting in upregulation of protective mechanisms (99). There are many other mechanisms by which mitochondrial function affects the aging process.

There were clearly observable changes in mitochondrial morphology with NOK senescence. At early stages of cell culture, perinuclear clustering was observed (Fig. 6.3). At later passages, mitochondria formed a fused, filamentous network throughout the cytoplasm (Fig. 8.1).

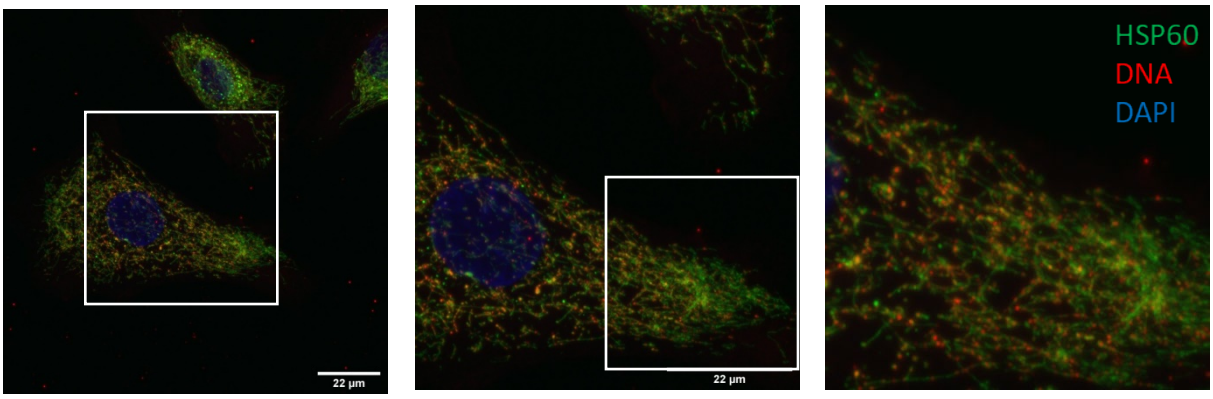

Figure. 8.1 NOK mitochondria at passage 14. (NOK 1408). (63x magnification, zoom = 1 (left), 2 (center), and 4 (right)). The middle and right images show the boxed area in the image to their immediate left.

Mitochondrial hyperfusion has been observed as a reaction to stress or senescence (100). This phenomenon is thought to be a survival mechanism. It may increase resistance to apoptosis, render mitochondria too large to undergo mitophagy, allow normally separate mitochondria to

share resources (lipids, proteins, RNA, mtDNA), and/or improve metabolic efficiency (101). Hyperfusion has been observed to be followed by release of mitochondrial derived vesicles (MDVs) into the cytosol, which are thought to travel to the lysosome for degradation (101). However, MDVs may also fuse with the plasma membrane and release their contents extracellularly (102). As noted above, in Chapters 6 and 7, HSP60 and mtDNA were found associated with NOK EVs. Other proteins that primarily localize to the mitochondria were also found in significantly increased amounts with senescence in the EV pellet: peroxiredoxin 5, HSP10, and adenylate kinase 2 (Supp. File 5). Together, this suggests that senescent NOKs may secrete vesicles derived from mitochondria. Determination of the precise mechanism merits future exploration.

An intriguing change occurring with senescence in NOKs was a decline in production of the mitochondrial derived peptide (MDP) humanin. Mitochondria contain a circular genome with 37 genes that code for 2 ribosomal RNAs, 13 proteins of the electron transport chain, and 22 transfer RNAs. The two rRNAs are the 12S component, transcribed from the *MT-RNR1* gene, and the 16S, transcribed from the *MT-RNR2* gene. The *MT-RNR2* gene also contains an open reading frame that codes for a 24-amino acid peptide, the humanin MDP (103). An enzyme-linked immunoassay (ELISA) of whole-cell lysate showed that the quantity of humanin declined significantly from early to late passages in NOKs (Fig. 8.2).

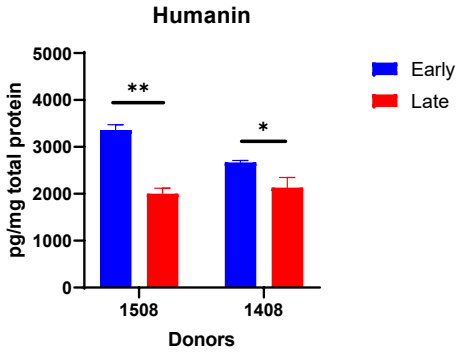

Figure 8.2 Humanin ELISA results. (Significance determined using t-test). *p<0.05, **p<0.01, ***p<0.001, ****p<0.0001.

Humanin has been found to have protective effects in aging (104). Some occur when humanin is secreted; however, humanin was not found in either the CM or EV pellet from NOKs, despite a search of the results for peptides with humanin-specific sequences, rather than relying solely on software to match mass spec-identified peptides to known protein sequences (email communication between R. Schwartz and A.-M. Pinto). It may be that humanin serves as a retrograde signal from mitochondria to the nucleus in NOKs (104). Fractionation of NOKs prior to an ELISA could be used to determine the subcellular locations of humanin.

Chapter 9 Concluding Discussion.

In this work, I have provided data in support of three overarching assertions of importance for senescence research. First, NOK senescence both overlaps with and is distinct from senescence in other cells. Second, the vesicular SASP deserves far more attention than it has received to date. Third, senescence in epithelial cells is strikingly similar, in many respects, to cancer in epithelial cells.

The identities between NOK senescence and that of other cells are apparent from the results of the assays showing that NOKs do senesce (Section 1.1), the RNA-seq data concerning key SASP elements and the immunoassay measurements of SASP components in conditioned medium (Section 4.1), and the mitochondrial hyperfusion (Chapter 8). A combination of similarities and differences is evidenced by the data concerning upregulation of inflammatory pathways (Sections 2.3, 2.4, and 4.2), and the partial (but not complete) overlap with a core signature of senescence (Section 2.6). A clear difference, compared to fibroblasts, is found in the presence of p21WAF1/CIP1 at early passages, and its decline with senescence, in NOKs (Section 1.2). Interestingly, even differences between donors were found within NOKs (Sections 2.2, 2.5, 5.2, and 5.3).

The content and role of EVs secreted by senescent cells can be expected to undergo closer scrutiny in the future. Proteomic analysis of NOK EVs showed significant increases in secretion of DAMPs and other molecules that can perpetrate chronic inflammation (Chapter 3, Section 4.3), and suggested a way in which senescent cells might undermine glycolysis, a metabolic process relied on by cancer cells (Section 3.2). Accordingly, I have proposed new SASP components associated with EVs (Chapter 6) and investigated the effect of EVs from senescent NOKs on one type of immune cells (Chapter 7). Although this work examined proteins and DNA, lipids and RNA will also be subjects of further investigation.

The similarity between senescent NOKs and cancer cells (Sections 2.1, 5.1, and 5.4) may initially seem unremarkable, given that senescence is a mechanism for preventing cancer and that some known senolytic treatments are anti-cancer drugs. However, it has a notable implication for cancer research. That is whether secretions attributed to cancer cells, and taken as biomarkers of cancer, might actually be secretions from senescent cells in patients who have received senescence-inducing therapy. Take, for example, a recently published proteomic analysis of EVs in which the authors concluded that they had identified biomarkers for cancer detection and determining cancer type (105). Some of the EV proteins identified as cancer biomarkers in that study (*e.g.,* tenascin, S100A13, basigin, cathepsin B, SERPINH1, integrin α5, and vimentin) also showed significant senescence-correlated increases in the EV pellets from NOKs (Supp. File 5). If the cancer patients from whom the samples used in the study were taken had received therapy that would induce senescence (such as radiation therapy directed to the tumor area), then there would likely be senescent cells in the tumor. But the composition of EVs from cells that had undergone therapy-induced senescence could not be used as markers to diagnose cancer in untreated patients.

Chapter 10 Future Directions

Scientific discovery is not unlike the mythological Hydra: multiple new lines of inquiry usually emerge for each question answered. (To extend the simile, research does often feel like a Herculean task.) This work is no exception. Two areas in particular recommend themselves to more in-depth study: (1) an identification of which EVs from senescent cells cause or exacerbate specific diseases and dysfunctions of aging and what treatments will be effective, and (2) a better understanding of the mechanisms by which senescent cells evade the immune system and how they can be safely overcome. An important element of both of these investigations will be whether the answers differ depending on some characteristic of the subjects (*e.g.,* sex).

The first question can be approached by isolating EVs (*e.g.,* from serum or cerebrospinal fluid) from individuals with a serious condition associated with aging, and comparing them to EVs from healthy aged and young individuals. Differences in protein, lipid, and nucleic acid content between bulk EVs from the groups of subjects can be identified. The next step would be to use those differences to identify particular EV populations that are specific to subjects suffering from the condition. This could be done by isolating EVs bearing a surface marker found exclusively (or highly enriched) in the subjects with the condition of interest. One method would be to use biotinylated antibodies to the marker that can be bound to streptavidin beads and incubated with the EVs, followed by FACS and elution of the EVs from the beads, with ensuing characterization of EV contents. Understanding how those EVs interact with other cells (whether they bind receptors on and/or are taken up by those other cells) and the effects on the target cells would then give insight into how they might be causing detrimental effects. Finally, it will be important to identify the source cells for these EVs, and whether those cells are senescent, in order to determine which cells should be targeted for elimination.

The second question focuses on how that elimination can be implemented, and the answers include leveraging of the immune system and its interactions with senescent cells. Although these strategies can be applied in conjunction with the EV identification strategy just described, they can also be employed independently of it, when deleterious senescent cells are identified through other means. If a surface marker for the problematic cells is absent from other, essential cells in the organism, the cell to be destroyed can be targeted in a way that attracts NK and/or CD+8 T cells. NK cells can engage in antibody dependent cellular cytotoxicity against senescent cells bearing a specific protein on their surface when antibodies to the protein are supplied exogenously in order to coat those cells (47). Alternatively, chimeric antigen receptor (CAR) T and CAR NK cells have been used to eliminate cancer cells (106), and can also be engineered to destroy senescent cells (39). If the surface protein is one that is also present on healthy cells that should be preserved, and if the surface protein participates in immune evasion (rather than simply serving as a marker), a better approach could be use of an antibody to temporarily and locally counteract its immune suppressive effects. This may restore the vigor of the organism's NK and CD8+ T cells, so that they can perform their function of eliminating senescent cells. CD73, discussed in Chapter 5, appears to be an example of this. CD73 is normally expressed on healthy vascular endothelial cells (107), destruction of which it presumably would be preferable to avoid. A number of clinical trials are studying anti-CD73 antibody use in cancer (https://www.cancer.gov/about-cancer/treatment/clinical-trials/intervention/anti-cd73-monoclonal-antibody-medi9447) and (https://www.cancer.gov/about-cancer/treatment/clinical-trials/intervention/anti-cd73-monoclonal-antibody-bms-986179). The use of antibodies to CD73 for elimination of senescent cells may present another opportunity for repurposing of an anti-cancer therapy (similar to adaptation of Bcl-2 family inhibitors to senolytic ends). Conversely, senolytics developed to remove senescent cells that accumulate with age can also be used to eliminate senescent cells that result from use of certain cancer therapies (*e.g.,* chemotherapy, radiation, CDK4/6 inhibitors) (108).

With the aging of the global population, the need to address health conditions that afflict this demographic segment will continue to grow. Elimination of senescent cells, or amelioration of their effects, can extend healthspan, improving quality of life and reducing the cost of care burden. Before this can be accomplished, we must understand more about how senescence operates. The goal of this work has been to add to that body of knowledge.

METHODS

Cell culture

NOKs were collected at the National Institutes of Health during third molar extractions and isolated according to published procedures (24). NOKs were cultured on surfaces coated with collagen I protein (Gibco #A1048301) in Defined Keratinocyte Serum-Free Medium (DKSFM) (Life Technologies #10744019) with penicillin-streptomycin (Gibco #15140163). $5x10^5$ cells were plated in a 10 cm dish in 10 mL of DKSFM and passaged every 4 days through passage 11 and every 5 days thereafter to determine growth rates. Medium was replaced at 48 hours after passaging and was replaced or cells were passaged at 96 hours. Collected medium was centrifuged for 5 minutes at 1500 x g. Supernatant was transferred to fresh tubes and stored at -80°C. All cells used tested negative for mycoplasma using the MycoAlert Mycoplasma Detection Kit (Lonza #LT07-318).

RNA-seq

10^5 NOKs were plated in each of 2 wells of a 6-well plate and grown for 5 days. Cells were collected in TRIzol (Life Technologies #15596026) and stored at -80°C. RNA was extracted using the Direct-zol RNA Miniprep kit (Zymo Research #R2050). Quality of isolated total RNA was assessed using Agilent TapeStation 4200. RNA-Seq libraries were prepared using the TruSeq Total mRNA Sample Preparation Kit (Illumina). RNA-seq libraries were multiplexed, normalized, pooled for sequencing, and sequenced on the HiSeq 2500 system (Illumina) at single read 50. Image analysis and base calling was done with Illumina CASAVA-1.8.2.

RT-qPCR

cDNA was prepared from 1 µg of RNA (same samples used for RNA-seq) in a 20 µl reaction using qScript cDNA SuperMix (Quanta #84034). cDNA was diluted 1:10 in TE buffer.

qPCR was performed with 2.5 µl cDNA in a 20µl reaction using Power SYBR Green PCR Master Mix (Applied Biosystems #436789) and the following primers:

IL1α FP	AGTGCTGCTGAAGGAGATGCCTGA
IL1α RP	CCCCTGCCAAGCACACCCAGTA
IL1β FP	TGCACGCTCCGGGACTCACA
IL1β RP	CATGGAGAACACCACTTGTTGCTCC
IL6 FP	CCAGGAGCCCAGCTATGAAC
IL6 RP	CCCAGGGAGAAGGCAACTG
IL8 FP	GAGTGGACCACACTGCGCCA
IL8 RP	TCCACAACCCTCTGCACCCAGT
MMP1 FP	ATCGGCCCACAAACCCCAAA
MMP1 RP	TGGCAGTTGTGGCCAGAAAACA

Each sample was run in triplicate on a BioRad CFX384 Real Time machine as follows: 50°C for 2 minutes, 95°C for 10 minutes, and 40 cycles of 95°C for 15 seconds followed by 60°C for 1 minute.

Senescence associated β-galactosidase

NOKs were stained for SA β-gal (BioVision #K320-250) 4 days after passaging. Etoposide-treated (20 µM for 48 hours) BJ fibroblasts were the positive control. Cells were imaged 40 hours after application of stain. At least 500 cells were counted at each passage for each of four replicates.

EdU and FxCycle Violet

Cells were stained using the Click-iT EdU Flow Cytometry Assay Kit (Invitrogen #C10424), and FxCycle Violet Stain (Invitrogen #F10347). Treated cells were incubated with 10 µM EdU for 24 hours. U2OS cells were the positive control. NOKs not treated with EdU were the negative control. Cells were analyzed on a Becton-Dickinson LSRII flow cytometer. Results were plotted using FlowJo v10 software (FlowJo LLC).

γH2AX

NOKs were stained with an AF488-conjugated antibody (Cell Signaling Technology #9719) at a 1:1500 dilution and DAPI (ThermoFisher #D1306) per a published protocol (109). Etoposide-treated (2 μM for 48 hours) U2OS cells were the positive control. Images were acquired with a Zeiss 880 confocal (63x objective, zoom = 2). Images were randomized to perform manual scoring blind to passage number. At least 200 cells from each of passages 5 and 13 were scored.

Immunofluorescence for cyclin-dependent kinase inhibitors, HSP60, and Rad51

NOKs were cultured in 4-well collagen-coated glass slides (Millicell PEZGS0416). Cells were fixed with 4% paraformaldehyde and permeabilized with 0.2% Triton/3% FBS in PBS. Antibodies to p16INK4a (R&D Systems #AF5779), p21CIP1/WAF1 (ThermoFisher #MA5-14949), HSP60 (Cell Signaling Technology #12165S), and Rad51 (Abcam #63801) and secondary antibodies conjugated to AF647 (Invitrogen #A-21447) for p16 and AF488 (Invitrogen #A-21202 and #A-21206) for p21, HSP60, and Rad51 were used, as well as DAPI (ThermoFisher #D1306). Phalloidin conjugated to AF568 (ThermoFisher #A12379) was used to stain for actin. Slides were mounted using ProLong Glass Antifade Mountant (Invitrogen #P36980) and Slip-Rite Cover Glass (Thermo Scientific #152250). Positive staining for p21 at an early passage was confirmed using a second primary antibody (Cell Signaling Technology #2947). Etoposide-treated (2 μM for 48 hours) U2OS cells were the positive control for p21 and Rad51, and etoposide-treated (20μM for 48 hours) BJ fibroblasts were the positive control for p16. p16INK4a and Rad51 fluorescence were quantified using ImageJ.

Immunoblotting

Cells were washed with PBS and collected in RIPA buffer with protease/phosphatase inhibitor (Cell Signaling Technologies #55872S). Protein quantification was performed using Bio-

Rad DC Protein Assay reagents (Bio-Rad # 5000113, #5000114, and #5001155); readings were made on an Infinite M200 Pro plate reader (TECAN) at 750 nm. Protein content was normalized to the lowest concentration sample using the same buffer. Samples were prepared for immunoblotting with NuPAGE Sample Reducing Agent (Invitrogen #169323) and NuPAGE LDS Sample Buffer (Invitrogen #1771559), heated for 15 minutes at 70° C. Samples were run on NuPAGE 4-12% Bis-Tris gels (Invitrogen #NP0322BOX) using MOPS running buffer (Invitrogen #NP000102). Transfers were run using NuPAGE transfer buffer (Invitrogen #NP00061) onto nitrocellulose membranes (Thomas Scientific #1182G93). After transfer, Ponceau S staining was performed using 10x Ponceau S solution (0.5% (w/v) Ponceau S powder (Sigma-Aldrich #P3504) dissolved in 1% (v/v) glacial acetic acid) that had been diluted to 1x with sterile H20. Ponceau S stain was removed by incubating the stained membrane in 0.1N NaOH followed by washing in H2O. Membranes were blocked in TBST with 5% milk (American Bio AB10109-01000) and probed using antibodies to p21WAF1/CIP1 (Cell Signaling Technology #2947S), E2F1 (Santa Cruz Technology #SC-251), phosphorylated p-65 (S536) (Cell Signaling Technology #3033S), or β-actin conjugated to HRP (Cell Signaling Technology #5125S), overnight at 4°C in blocking buffer. For primary antibodies not conjugated to HRP, anti-rabbit or anti-mouse secondary antibodies so conjugated were used (Bio-Rad #1706515 and #170516) for one hour at room temperature in blocking buffer. Membranes were treated with Lumina Forte HRP Substrate (Millipore Sigma # WBLUF0100) and imaged on a ChemiDoc MP imaging system (BioRad). Bands were quantified using ImageJ.

Cytokine analysis

Medium was collected at 96 hours after passaging. Analysis was performed by Eve Technologies (Array #HD42) using a multiplex immunoassay kit (Millipore Sigma #HCYTMAG60PMX41BK) and analyzed with a Bio-Plex 200 system (Bio-Rad). Results were normalized for cell number and the amount of each protein present in clean DKSFM.

EV isolation for proteomics

Frozen CM was thawed on ice, centrifuged at 300 x g for 5 minutes at 4°C and then 2,000 x g for 10 minutes at 4°C. The supernatant was transferred to fresh tubes and centrifuged at 10,000 x g for 30 minutes at 4°C. 500 µL of medium was taken as the CM sample. The remainder was filtered through a 200 nm pore nylon filter (Pall Corp. #PN4433) and centrifuged in an Optima L-80XP using an SW-32 Ti rotor (Beckman Coulter) at 100,000 x g for 70 minutes at 4°C; the pellet was washed with ice-cold PBS, and centrifuged at 100,000 x g for 70 minutes at 4°C. Supernatant was removed and the pellet and CM sample were stored at -80°C.

Mass spectrometry

Samples were precipitated by methanol/chloroform and redissolved in 8 M urea/100 mM TEAB, pH 8.5. Proteins were reduced with 5 mM tris(2-carboxyethyl)phosphine hydrochloride (TCEP) (Sigma-Aldrich) and alkylated with 10 mM chloroacetamide (Sigma-Aldrich). Proteins were digested overnight at 37° C in 2 M urea/100 mM TEAB, pH 8.5, with trypsin (Promega). Digestion was quenched with formic acid, 5% final concentration. The digest was injected directly onto a 30 cm, 75 µm ID column packed with BEH 1.7um C18 resin (Waters). Samples were separated at a flow rate of 200 nl/min on a nLC 1000 (Thermo). Buffer A and B were 0.1% formic acid in water and 0.1% formic acid in 90% acetonitrile, respectively. A gradient of 1-25% Buffer B over 110 minutes, an increase to 40% Buffer B over 10 minutes, an increase to 90% Buffer B over 10 minutes and held at 90% Buffer B for a final 10 minutes was used for 140 minutes total run time. Column was re-equilibrated with 15 µl of Buffer A prior to the injection of sample. Peptides were eluted directly from the tip of the column and nanosprayed directly into the mass spectrometer by application of 2.5 kV voltage at the back of the column. Samples were analyzed on a Fusion Orbitrap tribrid mass spectrometer (Thermo). The Orbitrap Fusion was operated in a data dependent mode. Full MS scans were collected in the Orbitrap at 120K resolution with a mass range of 400 to 1500 m/z and an AGC target of 4e5. The cycle time was set to 3 seconds,

and within the 3 seconds the most abundant ions per scan were selected for CID MS/MS in the ion trap with an AGC target of 1e4 and minimum intensity of 5000. Maximum fill times were set to 50 ms and 100 ms for MS and MS/MS scans respectively. Quadrupole isolation at 1.6 m/z was used, monoisotopic precursor selection was enabled and dynamic exclusion was used with exclusion duration of 5 sec. Protein and peptide identification were done with Integrated Proteomics Pipeline – IP2 (Integrated Proteomics Applications). Tandem mass spectra were extracted from raw files using RawConverter and searched with ProLuCID against Uniprot human database. The search space included all fully-tryptic and half-tryptic peptide candidates. Carbamidomethylation on cysteine was considered as a static modification. Data was searched with 50 ppm precursor ion tolerance and 600 ppm fragment ion tolerance. Identified proteins were filtered using DTASelect and utilizing a target-decoy database search strategy to control the false discovery rate to 1% at the protein level. Normalized spectral abundance factor (NSAF) was calculated as the number of spectral counts (SpC) identifying a protein divided by the protein's length (L), divided by the sum of SpC/L for all proteins in the experiment.

Transmission electron microscopy

Exosomes isolated by ultracentrifugation were prepared for TEM using a published protocol (110). Fresh exosomes were negatively stained using 1% aqueous uranyl acetate for 1 minute. Exosomes fixed with 2% PFA were transferred to carbon-coated nickel grids, incubated with primary antibodies to CD9 (ThermoFisher #10626D), CD81 (ThermoFisher #10630D), or HSP60 (Cell Signaling Technology #12165S) at a concentration of 10 μg/μL. Secondary antibodies conjugated to 10 nm gold beads were donkey anti-mouse IgG (Electron Microscopy Sciences #25813) for CD9 and CD81 and goat anti-rabbit IgG (Electron Microscopy Sciences #25365) for HSP60. Images were acquired using a Leo Libra 120kV Transmission Electron Microscope (Carl Zeiss) equipped with a Gatan 4k 895-Ultrascan CCD camera, operated at 80 kV using Zero-loss imaging to increase contrast.

THP-1 cell co-incubation

Frozen CM from the final or penultimate passages from each donor was thawed on ice, centrifuged at 300 x g for 5 minutes at 4°C and 2,000 x g for 10 minutes at 4°C. Supernatant was transferred to fresh tubes and centrifuged at 10,000 x g for 30 minutes at 4°C. Supernatant from this last centrifugation step was filtered through a 200 nm pore nylon filter (Pall Corp. #PN4433). EVs were isolated using the qEV10/35nm size exclusion column (Izon). Fractions were analyzed using a NanoSight NS300 with NTA 3.1 software (Malvern Panalytical), then concentrated 8:1 by centrifuging at 3220 x g in Amicon® Ultra-15 3K filters (Millipore #UFC900308). Protein content was determined as for immunoblot samples. THP-1 Dual Reporter cells (InvivoGen #thpd-nfis) were cultured in RPMI1640 (ThermoFisher 11875093) with Glutamax (Gibco 35050-061), HEPES (Gibco # 15630130), 10% FBS (Gibco 10437-028) heat-inactivated at 56°C for 30 minutes, 100 µg/ml Normocin (InvivoGen #ant-nr-1), and penicillin-streptomycin (Gibco #15140163). Blasticidin (InvivoGen #ant-bl-1) at 10 µg/ml and Zeocin (InvivoGen #ant-zn-1) at 100 µg/ml were added to the medium at alternate passages for selection. THP-1 cells were plated (1.5 x 105/well in a 24-well plate) in 500 µl medium. 5 µg of EVs in sterile PBS were added to treated wells; an equal amount of sterile PBS was added to negative control wells. For the positive control, poly (dA:dT) complexed with LyoVec (InvivoGen #tlrl-piclv) was added to a final concentration of 100 ng/ml. H-161 (Invivogen #inh-h151) was used at a concentration of 500 ng/mL added every 24 hours, starting one hour before addition of EVs. Secretion of luciferase was detected using Quanti-Luc (InvivoGen #rep-qlc). Readings were performed using the luminescence function of the Infinite M200 Pro plate reader (TECAN) with a read time of 100 milliseconds.

DNA Extraction and sequencing

DNA was extracted from EVs using XCF Exosomal DNA Isolation Kit (System Biosciences #XCF200A-1) according to manufacturer’s protocol. Library preparation was performed using Nextera XT DNA kit (Illumina #FC-131-1096) according to the manufacturer's instructions and

DNA libraries were sequenced on NextSeq500 System (Illumina) using the mid-output kit at paired-end 75bp configuration.

Droplet digital PCR (ddPCR)

ddPCR was carried out using the QX-200 system (Bio-Rad) according to the manufacturer's user guides. Samples were prepared using 11 µL of ddPCR Supermix for Probes (no UTP) (Bio-Rad #1863023), 1.1 µL of 20x target primers/probe (Bio-Rad # 10031276), 330 ng DNA, and UltraPure DNase/RNase-Free Distilled Water (Gibco # 10977015) to a total volume of 22 µL, of which 20 µL was used for each reaction. A reaction with no DNA template was used as negative control and cDNA made from mRNA from passage 5 and last passage whole cells was used as positive control. Primer and probe sequences used are as follows:

ND1 FP	CCCTAAAACCCGCCACATCT
ND1 RP	GAGCGATGGTGAGAGCTAAGGT
ND1 probe	CCATCACCCTCTACATCACCGCCC

Enzyme-Linked Immunosorbent Assay (ELISA) for humanin

Late ELISA samples were last passage cells; early samples were from passages 5 through 7. Cells were washed with PBS and collected in RIPA buffer with 0.5M EDTA (Quality Biological #351-07-101) diluted 1:100 and protease/phosphatase inhibitor cocktail (Cell Signaling Technologies #55872S) diluted 1:100. Protein quantification was performed using Bio-Rad DC Protein Assay reagents A, B, and S (Bio-Rad #5000113, #5000114, and #5001155) according to manufacturer's instructions and readings were made using an Infinite M200 Pro plate reader (TECAN) at 750 nm. ELISAs were then performed by Dr. Junxiang Wan, University of Southern California. Larger proteins were removed from the lysate using a solution of 90% acetonitrile and 10% 1N HCl; this mixture was centrifuged and the supernatant was transferred to a clean 1.5 ml tube and dried down by SpeedVac. The dried extract was reconstituted with PBST and used for

the ELISA (100 µg total protein per replicate). The ELISA plate was coated with capture antibody in 50 mM sodium bicarbonate buffer on a shaker for 4 hours. The plates were washed 2 times with wash buffer and 2 times with SuperBlock buffer (ThermoFisher #37515). Standards (synthetic peptide in a range of 50 pg/ml to 50,000 pg/ml) and extracted samples were added with pre-titered detection antibody and incubated overnight on a shaker. The plate was washed, and streptavidin-HRP conjugate was added and incubated for 30 minutes at room temperature. The plate was again washed and incubated with ultra-sensitive TMB and incubated for 10-20 minutes. The stop solution was added and the plate was read at 450 nm. Custom capture and detection antibodies to humanin and SHLP2 were produced by Harlan Laboratories (Indianapolis, IN), as previously described in Cobb L., *et al.* (103).

Bioinformatics

For RNA-seq, sequenced reads were quality-tested using FASTQC (https://www.bioinformatics.babraham.ac.uk/projects/fastqc/) v0.11.8 and aligned to the hg19 human genome using the STAR aligner version 2.5.3a. Mapping was carried out using default parameters, filtering non-canonical introns and allowing up to 10 mismatches per read and only keeping uniquely mapped reads. The genome index was constructed using the gene annotation supplied with the hg19 Illumina iGenomes collection (iGenomes online. Illumina. 2015. http://support.illumina.com/sequencing/sequencing_software/igenome.html) and sjdbOverhang value of 100. Raw or FPKM (fragments per kilobase per million mapped reads) gene expression was quantified across all gene exons with HOMER v4.10.4 analyzeRepeats.pl with hg19 annotation v6.4 and parameters -strand + -count exons -condenseGenes (top-expressed isoform as proxy for gene expression), and differential gene expression was carried out on the raw counts with HOMER getDiffExpression.pl that runs DESeq2 v1.14.1 using replicates to compute within-group dispersion and experimental batch modeled as a separate variable. Principal Component Analysis (PCA) was carried out on normalized filtered gene counts using the R prcomp function.

Motif enrichment analysis and motif searching was carried out with default HOMER findMotifs.pl with 1000 replicates for FDR calculations.

Overrepresentation analysis was carried out with WebGestalt, using the GO biological process non-redundant database with FDR < 0.01 as the significance threshold, protein coding genes as the reference list, a maximum number of genes in a category of 200, using a weighted set cover algorithm to minimize the number of significant terms to 10.

Differential proteomics analysis was carried out using trended robust empirical Bayes testing from the limma R package version 3.38.3 on preprocessed protein counts (NSAF corrected for cell number, log2 transformed, and filtered for mean expression > 0.0001, resulting in 915 proteins tested) and accounting for batch effects between experiment batches.

For DNA sequencing, samples were mapped to the hg38 human genome using STAR v2.5.3a and the non-repeat sequences were used to quantify the length-normalized coverage of reads across each chromosome. Since samples represent technical replicates, the aligned reads were merged with samtools v1.9. The total number of reads aligning to each chromosome, and the repeat-masked genome length (with repeat sequences removed), were used to calculate the normalized read count for each chromosome.

REFERENCES

1. Chandler H, Peters G. Stressing the cell cycle in senescence and aging. Curr Opin Cell Biol. 2013;25(6):765-71. Epub 2013/08/07. doi: 10.1016/j.ceb.2013.07.005. PubMed PMID: 23916530.

2. Prata L, Ovsyannikova IG, Tchkonia T, Kirkland JL. Senescent cell clearance by the immune system: Emerging therapeutic opportunities. Semin Immunol. 2018;40:101275. Epub 2019/05/16. doi: 10.1016/j.smim.2019.04.003. PubMed PMID: 31088710; PMCID: PMC7061456.

3. Lecot P, Alimirah F, Desprez PY, Campisi J, Wiley C. Context-dependent effects of cellular senescence in cancer development. Br J Cancer. 2016;114(11):1180-4. Epub 2016/05/04. doi: 10.1038/bjc.2016.115. PubMed PMID: 27140310; PMCID: PMC4891501.

4. Kale A, Sharma A, Stolzing A, Desprez PY, Campisi J. Role of immune cells in the removal of deleterious senescent cells. Immun Ageing. 2020;17:16. Epub 2020/06/11. doi: 10.1186/s12979-020-00187-9. PubMed PMID: 32518575; PMCID: PMC7271494.

5. Campisi J. Aging, cellular senescence, and cancer. Annu Rev Physiol. 2013;75:685-705. Epub 2012/11/13. doi: 10.1146/annurev-physiol-030212-183653. PubMed PMID: 23140366; PMCID: PMC4166529.

6. Wiley CD, Velarde MC, Lecot P, Liu S, Sarnoski EA, Freund A, Shirakawa K, Lim HW, Davis SS, Ramanathan A, Gerencser AA, Verdin E, Campisi J. Mitochondrial Dysfunction Induces Senescence with a Distinct Secretory Phenotype. Cell Metab. 2016;23(2):303-14. doi: 10.1016/j.cmet.2015.11.011. PubMed PMID: 26686024; PMCID: PMC4749409.

7. Martinez-Zamudio RI, Robinson L, Roux PF, Bischof O. SnapShot: Cellular Senescence Pathways. Cell. 2017;170(4):816- e1. Epub 2017/08/13. doi: 10.1016/j.cell.2017.07.049. PubMed PMID: 28802049.

8. Kosar M, Bartkova J, Hubackova S, Hodny Z, Lukas J, Bartek J. Senescence-associated heterochromatin foci are dispensable for cellular senescence, occur in a cell type- and insult-dependent manner and follow expression of p16(ink4a). Cell Cycle. 2011;10(3):457-68. Epub 2011/01/21. doi: 10.4161/cc.10.3.14707. PubMed PMID: 21248468.

9. Sati S, Bonev B, Szabo Q, Jost D, Bensadoun P, Serra F, Loubiere V, Papadopoulos GL, Rivera-Mulia JC, Fritsch L, Bouret P, Castillo D, Gelpi JL, Orozco M, Vaillant C, Pellestor F, Bantignies F, Marti-Renom MA, Gilbert DM, Lemaitre JM, Cavalli G. 4D Genome Rewiring during Oncogene-Induced and Replicative Senescence. Mol Cell. 2020;78(3):522-38 e9. Epub 2020/03/30. doi: 10.1016/j.molcel.2020.03.007. PubMed PMID: 32220303; PMCID: PMC7208559.

10. He S, Sharpless NE. Senescence in Health and Disease. Cell. 2017;169(6):1000-11. Epub 2017/06/03. doi: 10.1016/j.cell.2017.05.015. PubMed PMID: 28575665; PMCID: PMC5643029.

11. Wang B, Kohli J, Demaria M. Senescent Cells in Cancer Therapy: Friends or Foes? Trends Cancer. 2020;6(10):838-57. Epub 2020/06/03. doi: 10.1016/j.trecan.2020.05.004. PubMed PMID: 32482536.

12. Milanovic M, Fan DNY, Belenki D, Dabritz JHM, Zhao Z, Yu Y, Dorr JR, Dimitrova L, Lenze D, Monteiro Barbosa IA, Mendoza-Parra MA, Kanashova T, Metzner M, Pardon K, Reimann M, Trumpp A, Dorken B, Zuber J, Gronemeyer H, Hummel M, Dittmar G, Lee S, Schmitt CA. Senescence-associated reprogramming promotes cancer stemness. Nature. 2018;553(7686):96-100. Epub 2017/12/21. doi: 10.1038/nature25167. PubMed PMID: 29258294.

13. Pereira BI, Devine OP, Vukmanovic-Stejic M, Chambers ES, Subramanian P, Patel N, Virasami A, Sebire NJ, Kinsler V, Valdovinos A, LeSaux CJ, Passos JF, Antoniou A, Rustin MHA, Campisi J, Akbar AN. Senescent cells evade immune clearance via HLA-E-mediated NK and CD8(+) T cell inhibition. Nat Commun. 2019;10(1):2387. doi: 10.1038/s41467-019-10335-5. PubMed PMID: 31160572; PMCID: PMC6547655.

14. Furman D, Campisi J, Verdin E, Carrera-Bastos P, Targ S, Franceschi C, Ferrucci L, Gilroy DW, Fasano A, Miller GW, Miller AH, Mantovani A, Weyand CM, Barzilai N, Goronzy JJ, Rando TA, Effros RB, Lucia A, Kleinstreuer N, Slavich GM. Chronic inflammation in the etiology of disease across the life span. Nat Med. 2019;25(12):1822-32. doi: 10.1038/s41591-019-0675-0. PubMed PMID: 31806905.

15. Cohen J, Torres C. Astrocyte senescence: Evidence and significance. Aging Cell. 2019;18(3):e12937. doi: 10.1111/acel.12937. PubMed PMID: 30815970; PMCID: PMC6516680.

16. Hernandez-Segura A, de Jong TV, Melov S, Guryev V, Campisi J, Demaria M. Unmasking Transcriptional Heterogeneity in Senescent Cells. Curr Biol. 2017;27(17):2652-60 e4. doi: 10.1016/j.cub.2017.07.033. PubMed PMID: 28844647; PMCID: PMC5788810.

17. Rossman MJ, Kaplon RE, Hill SD, McNamara MN, Santos-Parker JR, Pierce GL, Seals DR, Donato AJ. Endothelial cell senescence with aging in healthy humans: prevention by habitual exercise and relation to vascular endothelial function. Am J Physiol Heart Circ Physiol. 2017;313(5):H890-H5. doi: 10.1152/ajpheart.00416.2017. PubMed PMID: 28971843; PMCID: PMC5792201.

18. Sousa-Victor P, Gutarra S, Garcia-Prat L, Rodriguez-Ubreva J, Ortet L, Ruiz-Bonilla V, Jardi M, Ballestar E, Gonzalez S, Serrano AL, Perdiguero E, Munoz-Canoves P. Geriatric muscle stem cells switch reversible quiescence into senescence. Nature. 2014;506(7488):316-21. Epub 2014/02/14. doi: 10.1038/nature13013. PubMed PMID: 24522534.

19. Coppe JP, Desprez PY, Krtolica A, Campisi J. The senescence-associated secretory phenotype: the dark side of tumor suppression. Annu Rev Pathol. 2010;5:99-118. doi: 10.1146/annurev-pathol-121808-102144. PubMed PMID: 20078217; PMCID: PMC4166495.

20. Roy AL, Sierra F, Howcroft K, Singer DS, Sharpless N, Hodes RJ, Wilder EL, Anderson JM. A Blueprint for Characterizing Senescence. Cell. 2020;183(5):1143-6. Epub 2020/11/01. doi: 10.1016/j.cell.2020.10.032. PubMed PMID: 33128870.

21. Grosse L, Wagner N, Emelyanov A, Molina C, Lacas-Gervais S, Wagner KD, Bulavin DV. Defined p16(High) Senescent Cell Types Are Indispensable for Mouse Healthspan. Cell Metab. 2020. Epub 2020/06/03. doi: 10.1016/j.cmet.2020.05.002. PubMed PMID: 32485135.

22. Basisty N, Kale A, Jeon OH, Kuehnemann C, Payne T, Rao C, Holtz A, Shah S, Sharma V, Ferrucci L, Campisi J, Schilling B. A proteomic atlas of senescence-associated secretomes for aging biomarker development. PLoS Biol. 2020;18(1):e3000599. Epub 2020/01/17. doi:

10.1371/journal.pbio.3000599. PubMed PMID: 31945054; PMCID: PMC6964821 following competing interests: JC is a founder and shareholder of Unity Biotechnology, which develops senolytic drugs. All other authors have declared no competing interests.

23. Niklander S, Bandaru D, Lambert DW, Hunter KD. ROCK inhibition modulates the senescence-associated secretory phenotype (SASP) in oral keratinocytes. FEBS Open Bio. 2020;10(12):2740-9. Epub 2020/10/24. doi: 10.1002/2211-5463.13012. PubMed PMID: 33095981; PMCID: PMC7714064.

24. Iglesias-Bartolome R, Patel V, Cotrim A, Leelahavanichkul K, Molinolo AA, Mitchell JB, Gutkind JS. mTOR inhibition prevents epithelial stem cell senescence and protects from radiation-induced mucositis. Cell Stem Cell. 2012;11(3):401-14. Epub 2012/09/11. doi: 10.1016/j.stem.2012.06.007. PubMed PMID: 22958932; PMCID: PMC3477550.

25. Jang DH, Bhawal UK, Min HK, Kang HK, Abiko Y, Min BM. A transcriptional roadmap to the senescence and differentiation of human oral keratinocytes. J Gerontol A Biol Sci Med Sci. 2015;70(1):20-32. doi: 10.1093/gerona/glt212. PubMed PMID: 24398559.

26. Kang MK, Kameta A, Shin KH, Baluda MA, Kim HR, Park NH. Senescence-associated genes in normal human oral keratinocytes. Exp Cell Res. 2003;287(2):272-81. PubMed PMID: 12837283.

27. Baek JH, Lee G, Kim SN, Kim JM, Kim M, Chung SC, Min BM. Common genes responsible for differentiation and senescence of human mucosal and epidermal keratinocytes. Int J Mol Med. 2003;12(3):319-25. PubMed PMID: 12883647.

28. Chien Y, Scuoppo C, Wang X, Fang X, Balgley B, Bolden JE, Premsrirut P, Luo W, Chicas A, Lee CS, Kogan SC, Lowe SW. Control of the senescence-associated secretory phenotype by NF-kappaB promotes senescence and enhances chemosensitivity. Genes Dev. 2011;25(20):2125-36. Epub 2011/10/08. doi: 10.1101/gad.17276711. PubMed PMID: 21979375; PMCID: PMC3205583.

29. Soto-Gamez A, Demaria M. Therapeutic interventions for aging: the case of cellular senescence. Drug Discov Today. 2017;22(5):786-95. Epub 2017/01/24. doi: 10.1016/j.drudis.2017.01.004. PubMed PMID: 28111332.

30. Kalluri R, LeBleu VS. The biology, function, and biomedical applications of exosomes. Science. 2020;367(6478). Epub 2020/02/08. doi: 10.1126/science.aau6977. PubMed PMID: 32029601.

31. Correia-Melo C, Passos JF. Mitochondria: Are they causal players in cellular senescence? Biochim Biophys Acta. 2015;1847(11):1373-9. doi: 10.1016/j.bbabio.2015.05.017. PubMed PMID: 26028303.

32. West AP, Khoury-Hanold W, Staron M, Tal MC, Pineda CM, Lang SM, Bestwick M, Duguay BA, Raimundo N, MacDuff DA, Kaech SM, Smiley JR, Means RE, Iwasaki A, Shadel GS. Mitochondrial DNA stress primes the antiviral innate immune response. Nature. 2015;520(7548):553-7. doi: 10.1038/nature14156. PubMed PMID: 25642965; PMCID: PMC4409480.

33. Higuchi-Sanabria R, Frankino PA, Paul JW, 3rd, Tronnes SU, Dillin A. A Futile Battle? Protein Quality Control and the Stress of Aging. Dev Cell. 2018;44(2):139-63. Epub 2018/02/06. doi: 10.1016/j.devcel.2017.12.020. PubMed PMID: 29401418; PMCID: PMC5896312.

34. Sugiura A, McLelland GL, Fon EA, McBride HM. A new pathway for mitochondrial quality control: mitochondrial-derived vesicles. EMBO J. 2014;33(19):2142-56. doi: 10.15252/embj.201488104. PubMed PMID: 25107473; PMCID: PMC4282503.

35. Kirkland JL, Tchkonia T. Senolytic drugs: from discovery to translation. J Intern Med. 2020;288(5):518-36. Epub 2020/07/21. doi: 10.1111/joim.13141. PubMed PMID: 32686219; PMCID: PMC7405395.

36. Munoz DP, Yannone SM, Daemen A, Sun Y, Vakar-Lopez F, Kawahara M, Freund AM, Rodier F, Wu JD, Desprez PY, Raulet DH, Nelson PS, van 't Veer LJ, Campisi J, Coppe JP. Targetable mechanisms driving immunoevasion of persistent senescent cells link chemotherapy-resistant cancer to aging. JCI Insight. 2019;5. Epub 2019/06/12. doi: 10.1172/jci.insight.124716. PubMed PMID: 31184599; PMCID: PMC6675550.

37. Xu M, Pirtskhalava T, Farr JN, Weigand BM, Palmer AK, Weivoda MM, Inman CL, Ogrodnik MB, Hachfeld CM, Fraser DG, Onken JL, Johnson KO, Verzosa GC, Langhi LGP, Weigl M, Giorgadze N, LeBrasseur NK, Miller JD, Jurk D, Singh RJ, Allison DB, Ejima K, Hubbard GB, Ikeno Y, Cubro H, Garovic VD, Hou X, Weroha SJ, Robbins PD, Niedernhofer LJ, Khosla S, Tchkonia T, Kirkland JL. Senolytics improve physical function and increase lifespan in old age. Nat Med. 2018;24(8):1246-56. Epub 2018/07/11. doi: 10.1038/s41591-018-0092-9. PubMed PMID: 29988130; PMCID: PMC6082705.

38. Guerrero A, Herranz N, Sun B, Wagner V, Gallage S, Guiho R, Wolter K, Pombo J, Irvine EE, Innes AJ, Birch J, Glegola J, Manshaei S, Heide D, Dharmalingam G, Harbig J, Olona A, Behmoaras J, Dauch D, Uren AG, Zender L, Vernia S, Martinez-Barbera JP, Heikenwalder M, Withers DJ, Gil J. Cardiac glycosides are broad-spectrum senolytics. Nat Metab. 2019;1(11):1074-88. Epub 2019/12/05. doi: 10.1038/s42255-019-0122-z. PubMed PMID: 31799499; PMCID: PMC6887543.

39. Amor C, Feucht J, Leibold J, Ho YJ, Zhu C, Alonso-Curbelo D, Mansilla-Soto J, Boyer JA, Li X, Giavridis T, Kulick A, Houlihan S, Peerschke E, Friedman SL, Ponomarev V, Piersigilli A, Sadelain M, Lowe SW. Senolytic CAR T cells reverse senescence-associated pathologies. Nature. 2020;583(7814):127-32. Epub 2020/06/20. doi: 10.1038/s41586-020-2403-9. PubMed PMID: 32555459; PMCID: PMC7583560.

40. Scudellari M. To stay young, kill zombie cells. Nature. 2017;550(7677):448-50. Epub 2017/10/27. doi: 10.1038/550448a. PubMed PMID: 29072283.

41. Hernandez-Segura A, Nehme J, Demaria M. Hallmarks of Cellular Senescence. Trends Cell Biol. 2018;28(6):436-53. Epub 2018/02/27. doi: 10.1016/j.tcb.2018.02.001. PubMed PMID: 29477613.

42. Ogrunc M, d'Adda di Fagagna F. Never-ageing cellular senescence. Eur J Cancer. 2011;47(11):1616-22. Epub 2011/05/13. doi: 10.1016/j.ejca.2011.04.003. PubMed PMID: 21561762; PMCID: PMC3135819.

43. Dou Z, Ghosh K, Vizioli MG, Zhu J, Sen P, Wangensteen KJ, Simithy J, Lan Y, Lin Y, Zhou Z, Capell BC, Xu C, Xu M, Kieckhaefer JE, Jiang T, Shoshkes-Carmel M, Tanim K, Barber GN, Seykora JT, Millar SE, Kaestner KH, Garcia BA, Adams PD, Berger SL. Cytoplasmic chromatin triggers inflammation in senescence and cancer. Nature. 2017;550(7676):402-6. doi: 10.1038/nature24050. PubMed PMID: 28976970; PMCID: PMC5850938.

44. Stein GH, Drullinger LF, Soulard A, Dulic V. Differential roles for cyclin-dependent kinase inhibitors p21 and p16 in the mechanisms of senescence and differentiation in human fibroblasts. Mol Cell Biol. 1999;19(3):2109-17. doi: 10.1128/mcb.19.3.2109. PubMed PMID: 10022898; PMCID: PMC84004.

45. Karimian A, Ahmadi Y, Yousefi B. Multiple functions of p21 in cell cycle, apoptosis and transcriptional regulation after DNA damage. DNA Repair (Amst). 2016;42:63-71. Epub 2016/05/09. doi: 10.1016/j.dnarep.2016.04.008. PubMed PMID: 27156098.

46. Kang MK, Guo W, Park NH. Replicative senescence of normal human oral keratinocytes is associated with the loss of telomerase activity without shortening of telomeres. Cell Growth Differ. 1998;9(1):85-95. PubMed PMID: 9438392.

47. Kim KM, Noh JH, Bodogai M, Martindale JL, Yang X, Indig FE, Basu SK, Ohnuma K, Morimoto C, Johnson PF, Biragyn A, Abdelmohsen K, Gorospe M. Identification of senescent cell surface targetable protein DPP4. Genes Dev. 2017;31(15):1529-34. Epub 2017/09/08. doi: 10.1101/gad.302570.117. PubMed PMID: 28877934; PMCID: PMC5630018.

48. Brett JO, Arjona M, Ikeda M, Quarta M, de Morrée A, Egner IM, Perandini LA, Ishak HD, Goshayeshi A, Benjamin DI, Both P, Rodríguez-Mateo C, Betley MJ, Wyss-Coray T, Rando TA. Exercise rejuvenates quiescent skeletal muscle stem cells in old mice through restoration of Cyclin D1. Nature Metabolism. 2020;2(4):307-17. doi: 10.1038/s42255-020-0190-0.

49. Fleming JD, Pavesi G, Benatti P, Imbriano C, Mantovani R, Struhl K. NF-Y coassociates with FOS at promoters, enhancers, repetitive elements, and inactive chromatin regions, and is stereo-positioned with growth-controlling transcription factors. Genome Res. 2013;23(8):1195-209. Epub 2013/04/19. doi: 10.1101/gr.148080.112. PubMed PMID: 23595228; PMCID: PMC3730095.

50. Pao PC, Patnaik D, Watson LA, Gao F, Pan L, Wang J, Adaikkan C, Penney J, Cam HP, Huang WC, Pantano L, Lee A, Nott A, Phan TX, Gjoneska E, Elmsaouri S, Haggarty SJ, Tsai LH. HDAC1 modulates OGG1-initiated oxidative DNA damage repair in the aging brain and Alzheimer's disease. Nat Commun. 2020;11(1):2484. Epub 2020/05/20. doi: 10.1038/s41467-020-16361-y. PubMed PMID: 32424276; PMCID: PMC7235043.

51. Collin G, Huna A, Warnier M, Flaman JM, Bernard D. Transcriptional repression of DNA repair genes is a hallmark and a cause of cellular senescence. Cell Death Dis. 2018;9(3):259. doi: 10.1038/s41419-018-0300-z. PubMed PMID: 29449545; PMCID: PMC5833687.

52. Jackson DP, Ting JH, Pozniak PD, Meurice C, Schleidt SS, Dao A, Lee AH, Klinman E, Jordan-Sciutto KL. Identification and characterization of two novel alternatively spliced E2F1 transcripts in the rat CNS. Mol Cell Neurosci. 2018;92:1-11. doi: 10.1016/j.mcn.2018.06.003. PubMed PMID: 29936143; PMCID: PMC6191325.

53. Sullivan MR, Bernstein KA. RAD-ical New Insights into RAD51 Regulation. Genes (Basel). 2018;9(12). Epub 2018/12/16. doi: 10.3390/genes9120629. PubMed PMID: 30551670; PMCID: PMC6316741.

54. Wei Q, Cheng L, Amos CI, Wang LE, Guo Z, Hong WK, Spitz MR. Repair of tobacco carcinogen-induced DNA adducts and lung cancer risk: a molecular epidemiologic study. J Natl Cancer Inst. 2000;92(21):1764-72. Epub 2000/11/04. doi: 10.1093/jnci/92.21.1764. PubMed PMID: 11058619.

55. Gachechiladze M, Skarda J, Soltermann A, Joerger M. RAD51 as a potential surrogate marker for DNA repair capacity in solid malignancies. Int J Cancer. 2017;141(7):1286-94. Epub 2017/05/10. doi: 10.1002/ijc.30764. PubMed PMID: 28477336.

56. Huang J, Xie Y, Sun X, Zeh HJ, 3rd, Kang R, Lotze MT, Tang D. DAMPs, ageing, and cancer: The 'DAMP Hypothesis'. Ageing Res Rev. 2015;24(Pt A):3-16. Epub 2014/12/03. doi: 10.1016/j.arr.2014.10.004. PubMed PMID: 25446804; PMCID: PMC4416066.

57. Jeppesen DK, Fenix AM, Franklin JL, Higginbotham JN, Zhang Q, Zimmerman LJ, Liebler DC, Ping J, Liu Q, Evans R, Fissell WH, Patton JG, Rome LH, Burnette DT, Coffey RJ. Reassessment of Exosome Composition. Cell. 2019;177(2):428-45 e18. doi: 10.1016/j.cell.2019.02.029. PubMed PMID: 30951670; PMCID: PMC6664447.

58. Moreno-Gonzalo O, Fernandez-Delgado I, Sanchez-Madrid F. Post-translational add-ons mark the path in exosomal protein sorting. Cell Mol Life Sci. 2018;75(1):1-19. Epub 2017/10/29. doi: 10.1007/s00018-017-2690-y. PubMed PMID: 29080091.

59. Johnson ECB, Dammer EB, Duong DM, Ping L, Zhou M, Yin L, Higginbotham LA, Guajardo A, White B, Troncoso JC, Thambisetty M, Montine TJ, Lee EB, Trojanowski JQ, Beach TG, Reiman EM, Haroutunian V, Wang M, Schadt E, Zhang B, Dickson DW, Ertekin-Taner N, Golde TE, Petyuk VA, De Jager PL, Bennett DA, Wingo TS, Rangaraju S, Hajjar I, Shulman JM, Lah JJ, Levey AI, Seyfried NT. Large-scale proteomic analysis of Alzheimer's disease brain and cerebrospinal fluid reveals early changes in energy metabolism associated with microglia and astrocyte activation. Nat Med. 2020. Epub 2020/04/15. doi: 10.1038/s41591-020-0815-6. PubMed PMID: 32284590.

60. Zhan T, Rindtorff N, Boutros M. Wnt signaling in cancer. Oncogene. 2017;36(11):1461-73. Epub 2016/09/13. doi: 10.1038/onc.2016.304. PubMed PMID: 27617575; PMCID: PMC5357762.

61. Brack AS, Conboy MJ, Roy S, Lee M, Kuo CJ, Keller C, Rando TA. Increased Wnt signaling during aging alters muscle stem cell fate and increases fibrosis. Science. 2007;317(5839):807-10. Epub 2007/08/11. doi: 10.1126/science.1144090. PubMed PMID: 17690295.

62. Dovrat S, Caspi M, Zilberberg A, Lahav L, Firsow A, Gur H, Rosin-Arbesfeld R. 14-3-3 and beta-catenin are secreted on extracellular vesicles to activate the oncogenic Wnt pathway. Mol Oncol. 2014;8(5):894-911. doi: 10.1016/j.molonc.2014.03.011. PubMed PMID: 24721736; PMCID: PMC5528515.

63. Mastellos DC, Reis ES, Ricklin D, Smith RJ, Lambris JD. Complement C3-Targeted Therapy: Replacing Long-Held Assertions with Evidence-Based Discovery. Trends Immunol.

2017;38(6):383-94. doi: 10.1016/j.it.2017.03.003. PubMed PMID: 28416449; PMCID: PMC5447467.

64. Winck FV, Prado Ribeiro AC, Ramos Domingues R, Ling LY, Riano-Pachon DM, Rivera C, Brandao TB, Gouvea AF, Santos-Silva AR, Coletta RD, Paes Leme AF. Insights into immune responses in oral cancer through proteomic analysis of saliva and salivary extracellular vesicles. Sci Rep. 2015;5:16305. Epub 2015/11/06. doi: 10.1038/srep16305. PubMed PMID: 26538482; PMCID: PMC4633731.

65. Perkins A, Nelson KJ, Parsonage D, Poole LB, Karplus PA. Peroxiredoxins: guardians against oxidative stress and modulators of peroxide signaling. Trends Biochem Sci. 2015;40(8):435-45. Epub 2015/06/13. doi: 10.1016/j.tibs.2015.05.001. PubMed PMID: 26067716; PMCID: PMC4509974.

66. Mullen L, Hanschmann EM, Lillig CH, Herzenberg LA, Ghezzi P. Cysteine Oxidation Targets Peroxiredoxins 1 and 2 for Exosomal Release through a Novel Mechanism of Redox-Dependent Secretion. Mol Med. 2015;21:98-108. Epub 2015/02/26. doi: 10.2119/molmed.2015.00033. PubMed PMID: 25715249; PMCID: PMC4461588.

67. Orjalo AV, Bhaumik D, Gengler BK, Scott GK, Campisi J. Cell surface-bound IL-1alpha is an upstream regulator of the senescence-associated IL-6/IL-8 cytokine network. Proc Natl Acad Sci U S A. 2009;106(40):17031-6. doi: 10.1073/pnas.0905299106. PubMed PMID: 19805069; PMCID: PMC2761322.

68. Wang W, Mani AM, Wu ZH. DNA damage-induced nuclear factor-kappa B activation and its roles in cancer progression. J Cancer Metastasis Treat. 2017;3:45-59. doi: 10.20517/2394-4722.2017.03. PubMed PMID: 28626800; PMCID: PMC5472228.

69. Freund A, Patil CK, Campisi J. p38MAPK is a novel DNA damage response-independent regulator of the senescence-associated secretory phenotype. EMBO J. 2011;30(8):1536-48. doi: 10.1038/emboj.2011.69. PubMed PMID: 21399611; PMCID: PMC3102277.

70. Grunvogel O, Esser-Nobis K, Windisch MP, Frese M, Trippler M, Bartenschlager R, Lohmann V, Binder M. Type I and type II interferon responses in two human liver cell lines (Huh-7 and HuH6). Genom Data. 2016;7:166-70. Epub 2016/03/17. doi: 10.1016/j.gdata.2015.12.017. PubMed PMID: 26981398; PMCID: PMC4778650.

71. Wu Z, Oeck S, West AP, Mangalhara KC, Sainz AG, Newman LE, Zhang XO, Wu L, Yan Q, Bosenberg M, Liu Y, Sulkowski PL, Tripple V, Kaech SM, Glazer PM, Shadel GS. Mitochondrial DNA Stress Signalling Protects the Nuclear Genome. Nat Metab. 2019;1(12):1209-18. Epub 2020/05/13. doi: 10.1038/s42255-019-0150-8. PubMed PMID: 32395698; PMCID: PMC7213273 with regard to the data presented in the manuscript.

72. Weichselbaum RR, Ishwaran H, Yoon T, Nuyten DS, Baker SW, Khodarev N, Su AW, Shaikh AY, Roach P, Kreike B, Roizman B, Bergh J, Pawitan Y, van de Vijver MJ, Minn AJ. An interferon-related gene signature for DNA damage resistance is a predictive marker for chemotherapy and radiation for breast cancer. Proc Natl Acad Sci U S A. 2008;105(47):18490-5. Epub 2008/11/13. doi: 10.1073/pnas.0809242105. PubMed PMID: 19001271; PMCID: PMC2587578.

73. Swanson KV, Deng M, Ting JP. The NLRP3 inflammasome: molecular activation and regulation to therapeutics. Nat Rev Immunol. 2019;19(8):477-89. doi: 10.1038/s41577-019-0165-0. PubMed PMID: 31036962.

74. Cypryk W, Nyman TA, Matikainen S. From Inflammasome to Exosome-Does Extracellular Vesicle Secretion Constitute an Inflammasome-Dependent Immune Response? Front Immunol. 2018;9:2188. doi: 10.3389/fimmu.2018.02188. PubMed PMID: 30319640; PMCID: PMC6167409.

75. Gong T, Liu L, Jiang W, Zhou R. DAMP-sensing receptors in sterile inflammation and inflammatory diseases. Nat Rev Immunol. 2020;20(2):95-112. Epub 2019/09/29. doi: 10.1038/s41577-019-0215-7. PubMed PMID: 31558839.

76. Hartman ML, Czyz M. BCL-w: apoptotic and non-apoptotic role in health and disease. Cell Death Dis. 2020;11(4):260. Epub 2020/04/23. doi: 10.1038/s41419-020-2417-0. PubMed PMID: 32317622; PMCID: PMC7174325.

77. Chang J, Wang Y, Shao L, Laberge RM, Demaria M, Campisi J, Janakiraman K, Sharpless NE, Ding S, Feng W, Luo Y, Wang X, Aykin-Burns N, Krager K, Ponnappan U, Hauer-Jensen M, Meng A, Zhou D. Clearance of senescent cells by ABT263 rejuvenates aged hematopoietic stem cells in mice. Nat Med. 2016;22(1):78-83. doi: 10.1038/nm.4010. PubMed PMID: 26657143; PMCID: PMC4762215.

78. Vogler M. BCL2A1: the underdog in the BCL2 family. Cell Death Differ. 2012;19(1):67-74. doi: 10.1038/cdd.2011.158. PubMed PMID: 22075983; PMCID: PMC3252829.

79. Guerra RM, Bird GH, Harvey EP, Dharia NV, Korshavn KJ, Prew MS, Stegmaier K, Walensky LD. Precision Targeting of BFL-1/A1 and an ATM Co-dependency in Human Cancer. Cell Rep. 2018;24(13):3393-403 e5. Epub 2018/09/27. doi: 10.1016/j.celrep.2018.08.089. PubMed PMID: 30257201; PMCID: PMC6365304.

80. Sagiv A, Burton DG, Moshayev Z, Vadai E, Wensveen F, Ben-Dor S, Golani O, Polic B, Krizhanovsky V. NKG2D ligands mediate immunosurveillance of senescent cells. Aging (Albany NY). 2016;8(2):328-44. doi: 10.18632/aging.100897. PubMed PMID: 26878797; PMCID: PMC4789586.

81. Synowsky SA, Shirran SL, Cooke FGM, Antoniou AN, Botting CH, Powis SJ. The major histocompatibility complex class I immunopeptidome of extracellular vesicles. J Biol Chem. 2017;292(41):17084-92. doi: 10.1074/jbc.M117.805895. PubMed PMID: 28860189; PMCID: PMC5641862.

82. Jordier F, Gras D, De Grandis M, D'Journo XB, Thomas PA, Chanez P, Picard C, Chiaroni J, Paganini J, Di Cristofaro J. HLA-H: Transcriptional Activity and HLA-E Mobilization. Front Immunol. 2019;10:2986. Epub 2020/02/06. doi: 10.3389/fimmu.2019.02986. PubMed PMID: 32010122; PMCID: PMC6978722.

83. Pitti RM, Marsters SA, Lawrence DA, Roy M, Kischkel FC, Dowd P, Huang A, Donahue CJ, Sherwood SW, Baldwin DT, Godowski PJ, Wood WI, Gurney AL, Hillan KJ, Cohen RL, Goddard AD, Botstein D, Ashkenazi A. Genomic amplification of a decoy receptor for Fas ligand in lung and colon cancer. Nature. 1998;396(6712):699-703. doi: 10.1038/25387. PubMed PMID: 9872321.

84. Jenkins M, Keir M, McCune JM. A membrane-bound Fas decoy receptor expressed by human thymocytes. J Biol Chem. 2000;275(11):7988-93. doi: 10.1074/jbc.275.11.7988. PubMed PMID: 10713117.

85. LeBlanc HN, Ashkenazi A. Apo2L/TRAIL and its death and decoy receptors. Cell Death Differ. 2003;10(1):66-75. doi: 10.1038/sj.cdd.4401187. PubMed PMID: 12655296.

86. Manieri NA, Chiang EY, Grogan JL. TIGIT: A Key Inhibitor of the Cancer Immunity Cycle. Trends Immunol. 2017;38(1):20-8. Epub 2016/10/30. doi: 10.1016/j.it.2016.10.002. PubMed PMID: 27793572.

87. Vigano S, Alatzoglou D, Irving M, Menetrier-Caux C, Caux C, Romero P, Coukos G. Targeting Adenosine in Cancer Immunotherapy to Enhance T-Cell Function. Front Immunol. 2019;10:925. Epub 2019/06/28. doi: 10.3389/fimmu.2019.00925. PubMed PMID: 31244820; PMCID: PMC6562565.

88. Kordass T, Osen W, Eichmuller SB. Controlling the Immune Suppressor: Transcription Factors and MicroRNAs Regulating CD73/NT5E. Front Immunol. 2018;9:813. Epub 2018/05/04. doi: 10.3389/fimmu.2018.00813. PubMed PMID: 29720980; PMCID: PMC5915482.

89. Chigira M. Selfish cells in altruistic cell society - a theoretical oncology. Int J Oncol. 1993;3(3):441-55. Epub 1993/09/01. doi: 10.3892/ijo.3.3.441. PubMed PMID: 21573384.

90. Leclerc E, Fritz G, Vetter SW, Heizmann CW. Binding of S100 proteins to RAGE: an update. Biochim Biophys Acta. 2009;1793(6):993-1007. doi: 10.1016/j.bbamcr.2008.11.016. PubMed PMID: 19121341.

91. Li Y, Si R, Feng Y, Chen HH, Zou L, Wang E, Zhang M, Warren HS, Sosnovik DE, Chao W. Myocardial ischemia activates an injurious innate immune signaling via cardiac heat shock protein 60 and Toll-like receptor 4. J Biol Chem. 2011;286(36):31308-19. doi: 10.1074/jbc.M111.246124. PubMed PMID: 21775438; PMCID: PMC3173057.

92. Campanella C, Bucchieri F, Merendino AM, Fucarino A, Burgio G, Corona DF, Barbieri G, David S, Farina F, Zummo G, de Macario EC, Macario AJ, Cappello F. The odyssey of Hsp60 from tumor cells to other destinations includes plasma membrane-associated stages and Golgi and exosomal protein-trafficking modalities. PLoS One. 2012;7(7):e42008. doi: 10.1371/journal.pone.0042008. PubMed PMID: 22848686; PMCID: PMC3405006.

93. Cappello F, Conway de Macario E, Marino Gammazza A, Bonaventura G, Carini F, Czarnecka AM, Farina F, Zummo G, Macario AJ. Hsp60 and human aging: Les liaisons dangereuses. Front Biosci (Landmark Ed). 2013;18:626-37. doi: 10.2741/4126. PubMed PMID: 23276948.

94. Haag SM, Gulen MF, Reymond L, Gibelin A, Abrami L, Decout A, Heymann M, van der Goot FG, Turcatti G, Behrendt R, Ablasser A. Targeting STING with covalent small-molecule inhibitors. Nature. 2018;559(7713):269-73. Epub 2018/07/06. doi: 10.1038/s41586-018-0287-8. PubMed PMID: 29973723.

95. Lazaro-Ibanez E, Lasser C, Shelke GV, Crescitelli R, Jang SC, Cvjetkovic A, Garcia-Rodriguez A, Lotvall J. DNA analysis of low- and high-density fractions defines heterogeneous subpopulations of small extracellular vesicles based on their DNA cargo and topology. J Extracell

Vesicles. 2019;8(1):1656993. Epub 2019/09/10. doi: 10.1080/20013078.2019.1656993. PubMed PMID: 31497265; PMCID: PMC6719264.

96. Takahashi A, Okada R, Nagao K, Kawamata Y, Hanyu A, Yoshimoto S, Takasugi M, Watanabe S, Kanemaki MT, Obuse C, Hara E. Exosomes maintain cellular homeostasis by excreting harmful DNA from cells. Nat Commun. 2017;8:15287. Epub 2017/05/17. doi: 10.1038/ncomms15287. PubMed PMID: 28508895; PMCID: PMC5440838.

97. Malkin EZ, Bratman SV. Bioactive DNA from extracellular vesicles and particles. Cell Death Dis. 2020;11(7):584. Epub 2020/07/29. doi: 10.1038/s41419-020-02803-4. PubMed PMID: 32719324; PMCID: PMC7385258.

98. Riera CE, Merkwirth C, De Magalhaes Filho CD, Dillin A. Signaling Networks Determining Life Span. Annu Rev Biochem. 2016;85:35-64. Epub 2016/06/15. doi: 10.1146/annurev-biochem-060815-014451. PubMed PMID: 27294438.

99. Cox CS, McKay SE, Holmbeck MA, Christian BE, Scortea AC, Tsay AJ, Newman LE, Shadel GS. Mitohormesis in Mice via Sustained Basal Activation of Mitochondrial and Antioxidant Signaling. Cell Metab. 2018. doi: 10.1016/j.cmet.2018.07.011. PubMed PMID: 30122556.

100. Das R, Chakrabarti O. Mitochondrial hyperfusion: a friend or a foe. Biochem Soc Trans. 2020;48(2):631-44. Epub 2020/03/29. doi: 10.1042/BST20190987. PubMed PMID: 32219382.

101. Shutt TE, McBride HM. Staying cool in difficult times: mitochondrial dynamics, quality control and the stress response. Biochim Biophys Acta. 2013;1833(2):417-24. doi: 10.1016/j.bbamcr.2012.05.024. PubMed PMID: 22683990.

102. Picca A, Guerra F, Calvani R, Coelho-Junior HJ, Bossola M, Landi F, Bernabei R, Bucci C, Marzetti E. Generation and Release of Mitochondrial-Derived Vesicles in Health, Aging and Disease. J Clin Med. 2020;9(5). Epub 2020/05/16. doi: 10.3390/jcm9051440. PubMed PMID: 32408624; PMCID: PMC7290979.

103. Cobb LJ, Lee C, Xiao J, Yen K, Wong RG, Nakamura HK, Mehta HH, Gao Q, Ashur C, Huffman DM, Wan J, Muzumdar R, Barzilai N, Cohen P. Naturally occurring mitochondrial-derived peptides are age-dependent regulators of apoptosis, insulin sensitivity, and inflammatory markers. Aging (Albany NY). 2016;8(4):796-809. doi: 10.18632/aging.100943. PubMed PMID: 27070352; PMCID: PMC4925829.

104. Lee C, Yen K, Cohen P. Humanin: a harbinger of mitochondrial-derived peptides? Trends Endocrinol Metab. 2013;24(5):222-8. doi: 10.1016/j.tem.2013.01.005. PubMed PMID: 23402768; PMCID: PMC3641182.

105. Hoshino A, Kim HS, Bojmar L, Gyan KE, Cioffi M, Hernandez J, Zambirinis CP, Rodrigues G, Molina H, Heissel S, Mark MT, Steiner L, Benito-Martin A, Lucotti S, Di Giannatale A, Offer K, Nakajima M, Williams C, Nogues L, Pelissier Vatter FA, Hashimoto A, Davies AE, Freitas D, Kenific CM, Ararso Y, Buehring W, Lauritzen P, Ogitani Y, Sugiura K, Takahashi N, Aleckovic M, Bailey KA, Jolissant JS, Wang H, Harris A, Schaeffer LM, Garcia-Santos G, Posner Z, Balachandran VP, Khakoo Y, Raju GP, Scherz A, Sagi I, Scherz-Shouval R, Yarden Y, Oren M, Malladi M, Petriccione M, De Braganca KC, Donzelli M, Fischer C, Vitolano S, Wright GP, Ganshaw L, Marrano M, Ahmed A, DeStefano J, Danzer E, Roehrl MHA, Lacayo NJ, Vincent TC, Weiser MR, Brady MS, Meyers PA, Wexler LH, Ambati SR, Chou AJ, Slotkin EK, Modak S,

Roberts SS, Basu EM, Diolaiti D, Krantz BA, Cardoso F, Simpson AL, Berger M, Rudin CM, Simeone DM, Jain M, Ghajar CM, Batra SK, Stanger BZ, Bui J, Brown KA, Rajasekhar VK, Healey JH, de Sousa M, Kramer K, Sheth S, Baisch J, Pascual V, Heaton TE, La Quaglia MP, Pisapia DJ, Schwartz R, Zhang H, Liu Y, Shukla A, Blavier L, DeClerck YA, LaBarge M, Bissell MJ, Caffrey TC, Grandgenett PM, Hollingsworth MA, Bromberg J, Costa-Silva B, Peinado H, Kang Y, Garcia BA, O'Reilly EM, Kelsen D, Trippett TM, Jones DR, Matei IR, Jarnagin WR, Lyden D. Extracellular Vesicle and Particle Biomarkers Define Multiple Human Cancers. Cell. 2020;182(4):1044-61 e18. Epub 2020/08/17. doi: 10.1016/j.cell.2020.07.009. PubMed PMID: 32795414; PMCID: PMC7522766.

106. Li Y, Hermanson DL, Moriarity BS, Kaufman DS. Human iPSC-Derived Natural Killer Cells Engineered with Chimeric Antigen Receptors Enhance Anti-tumor Activity. Cell Stem Cell. 2018;23(2):181-92 e5. Epub 2018/08/08. doi: 10.1016/j.stem.2018.06.002. PubMed PMID: 30082067; PMCID: PMC6084450.

107. Niemela J, Henttinen T, Yegutkin GG, Airas L, Kujari AM, Rajala P, Jalkanen S. IFN-alpha induced adenosine production on the endothelium: a mechanism mediated by CD73 (ecto-5'-nucleotidase) up-regulation. J Immunol. 2004;172(3):1646-53. Epub 2004/01/22. doi: 10.4049/jimmunol.172.3.1646. PubMed PMID: 14734746.

108. Wang B, Kohli J, Demaria M. Senescent Cells in Cancer Therapy: Friends or Foes? Trends Cancer. 2020. Epub 2020/06/03. doi: 10.1016/j.trecan.2020.05.004. PubMed PMID: 32482536.

109. Noren Hooten N, Evans MK. Techniques to Induce and Quantify Cellular Senescence. J Vis Exp. 2017(123). doi: 10.3791/55533. PubMed PMID: 28518126; PMCID: PMC5565152.

110. Thery C, Amigorena S, Raposo G, Clayton A. Isolation and characterization of exosomes from cell culture supernatants and biological fluids. Curr Protoc Cell Biol. 2006;Chapter 3:Unit 3 22. doi: 10.1002/0471143030.cb0322s30. PubMed PMID: 18228490.